energies

MDPI

Review

Recent Progress and New Perspectives on Metal Amide and Imide Systems for Solid-State Hydrogen Storage

Sebastiano Garroni [1,*], Antonio Santoru [2], Hujun Cao [2], Martin Dornheim [2], Thomas Klassen [2,3], Chiara Milanese [4], Fabiana Gennari [5] and Claudio Pistidda [2,*]

1 International Research Centre in Critical Raw Materials—ICCRAM, Universidad de Burgos, Plaza Misael Banuelos s/n, 09001 Burgos, Spain
2 Institute of Materials Research, Materials Technology, Helmholtz-Zentrum Geesthacht GmbH, Max-Planck-Straße 1, 21502 Geesthacht, Germany; Antonio.Santoru@hzg.de (A.S.); Hujun.Cao@hzg.de (H.C.); martin.dornheim@hzg.de (M.D.); Thomas.Klassen@hzg.de (T.K.)
3 Department of Mechanical Engineering, Helmut Schmidt University, Holstenhofweg 85, Hamburg 22043, Germany
4 Pavia Hydrogen Lab, C.S.G.I. & Department of Chemistry, Physical-Chemistry Section, University of Pavia, Viale Taramelli, 16, 27100 Pavia, Italy; chiara.milanese@unipv.it
5 Centro Atómico Bariloche (CNEA) e Instituto Balseiro (UNCuyo), Bariloche, Río Negro R8402AGP, Argentina; gennari@cab.cnea.gov.ar
* Correspondence: sgarroni@ubu.es (S.G.); Claudio.Pistidda@hzg.de (C.P.); Tel.: +34-653-082-964 (S.G.); +49-(0)-4152-87-2644 (C.P.)

Received: 28 February 2018; Accepted: 19 April 2018; Published: 24 April 2018

Abstract: Hydrogen storage in the solid state represents one of the most attractive and challenging ways to supply hydrogen to a proton exchange membrane (PEM) fuel cell. Although in the last 15 years a large variety of material systems have been identified as possible candidates for storing hydrogen, further efforts have to be made in the development of systems which meet the strict targets of the Fuel Cells and Hydrogen Joint Undertaking (FCH JU) and U.S. Department of Energy (DOE). Recent projections indicate that a system possessing: (i) an ideal enthalpy in the range of 20–50 kJ/mol H_2, to use the heat produced by PEM fuel cell for providing the energy necessary for desorption; (ii) a gravimetric hydrogen density of 5 wt. % H_2 and (iii) fast sorption kinetics below 110 °C is strongly recommended. Among the known hydrogen storage materials, amide and imide-based mixtures represent the most promising class of compounds for on-board applications; however, some barriers still have to be overcome before considering this class of material mature for real applications. In this review, the most relevant progresses made in the recent years as well as the kinetic and thermodynamic properties, experimentally measured for the most promising systems, are reported and properly discussed.

Keywords: hydrogen storage materials; metal amides; thermodynamics and kinetics

1. Introduction

The constant growth in world population coupled with the rapid industrialization of the developing countries could lead to a drastic increase in the number of light-duty vehicles from now to 2050. Considering that the majority of the vehicles are currently based on the internal combustion engine (ICE) technology, the transportation sector is strongly dependent on petroleum-derived fuels which represent one of the biggest causes of carbon dioxide emission. In 2008, passenger cars were responsible for 17% of CO_2 emissions in the European Union. For these reasons, clean and

environmentally-friendly energy alternative carriers to the fossil fuels, capable of stabilizing global CO_2 level while sustaining the global mobility demand are desired. In this context, the "green" hydrogen fuel cell vehicles (FCVs) represent promising alternatives to the gasoline ICE. In order to achieve an extensive commercialization of hydrogen-powered cars, some obstacles have still to be overcome. Among them, the pressing issue is for on-board hydrogen storage in safe and efficient manner and, in this frame, hydrogen storage in solid state is considered as one of the most promising solution, as verified by the numerous studies all over the world focused on finding materials meeting the requirements for on-board applications established by the European Fuel Cell & Hydrogen Technology Platform and the US Department of Energy (DoE). For example, in proton exchange membrane fuel cells (PEMFC), hydrogen is supposed to be delivered under temperature below 90 °C, which implies the use materials with ΔH_{des} between 20–50 kJ/mol H_2 and ΔS_{des} between 100–130 J/(mol H_2 K) in order to reach 1 bar equilibrium hydrogen pressure.

Recently, many systems based on solid-state hydrogen storage materials have been tested in laboratory or on mobile prototypes. However, the parameters evaluated in laboratory tests were usually not suitable, in terms of gravimetric capacity and kinetics, for most light-duty passenger vehicles.

Since its discovery in 2002, the $LiNH_2$-LiH system [1] and in general amides and imides, have attracted more and more attentions as promising hydrogen storage materials, becoming one of the principal candidates for onboard applications on light-duty vehicles [2]. As shown in Figure 1, during the last 15 years, more than 300 among peer-reviewed papers and books have been published in the field of solid-state hydrogen storage, concerning this class of complex hydrides characterized by N-H bonds.

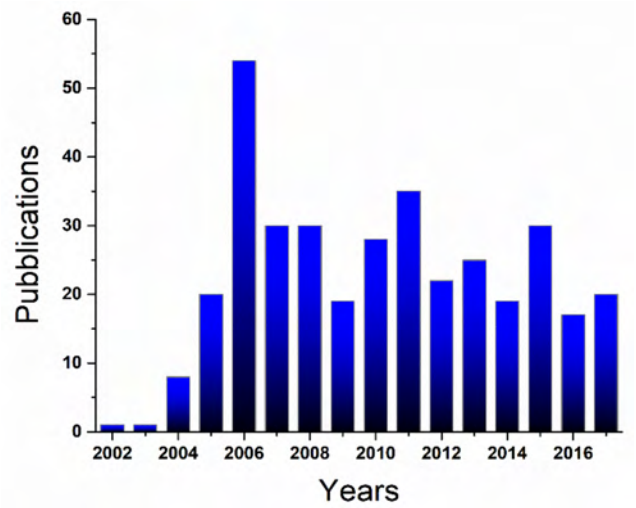

Figure 1. Number of publications on amides/imides compounds in the hydrogen storage field. Scopus sources. www.scopus.com.

From the picture in Figure 1, it is also possible to evince a constant and still actual fervent interest in amides/imides compounds for hydrogen storage purposes. This specific attention can be motivated by the fact that these systems can store sufficient amount of hydrogen in terms of gravimetric and volumetric densities, while possessing promising thermodynamic and kinetic properties with respect to the other classes of complex hydrides [2].

From a general and scientific point of view, most of the metal amide/imide systems exhibit endothermic hydrogen desorption with partial or full reversibility. Among them the $Mg(NH_2)_2$-2LiH composite possess high reversible hydrogen storage capacity (i.e., 5.0 wt. %) together with suitable thermodynamic properties (i.e., $\Delta H_{des} \approx 39$ kJ/mol H_2 and $\Delta S_{des} = 112$ J/mol H_2 K), optimal parameters for on-board application in fuel cell vehicles (FCVs). However, for technological applications, an important barrier is the poor kinetic rate during the dehydrogenation process. This is

mainly due to the high activation energy, which can be opportunely modulated by different approaches, including the addition of catalysts and the reduction the particle size. Also in this context, significant progresses have been made in the last years on the amides/imides systems, reducing the activation energy to ~80 kJ/mol, considered appealing for technological devices.

In this section, a detailed overview combined with the most recent progresses for different amides will be provided. Particular emphasis will be put on those systems with attractive features for practical applications.

2. Li-N-H System

One of the most interesting system, at present, is represented by the $LiNH_2$ + LiH mixture. When mixed, these substances show a reversible hydrogen storage capacity of 6.5 wt. % combined with a working temperature below 300 °C (285 °C) and appealing thermodynamic properties (ΔH_{des} = 45 kJ/mol) [1]. On the contrary, pure lithium amide and lithium hydride, separately, decompose at temperatures above 300 °C and 550 °C, respectively [3]. In the first desorption mechanism proposed, the driving force is represented by the release of hydrogen as a consequence of the direct reaction between the H^+ in $LiNH_2$ and H^- in LiH to form H_2 [4]. The second desorbing mechanism involves the decomposition of $LiNH_2$ to $\frac{1}{2}$ Li_2NH and $\frac{1}{2}$ NH_3 (Equation (1)), while, in the second step, $\frac{1}{2}$ LiH quickly reacts with $\frac{1}{2}$ NH_3 forming $\frac{1}{2}$ $LiNH_2$ and $\frac{1}{2}$ H_2 (Equation (2)) [5]:

$$LiNH_2 \leftrightarrow \frac{1}{2}\,Li_2NH + \frac{1}{2}\,NH_3 \tag{1}$$

$$\frac{1}{2}\,LiH + \frac{1}{2}\,NH_3 \leftrightarrow \frac{1}{2}\,LiNH_2 + \frac{1}{2}\,H_2 \tag{2}$$

Experimentally, in the temperature range of 180–400 °C this system desorbs hydrogen together with a large amount of ammonia, which should be avoided because it is the main responsible for the catalyst poisoning phenomenon in fuel cells [6–8]. Furthermore, it has been proved that the ammonia concentration brutally increases as the number of ab-desorption cycles increases, affecting the gravimetric capacity of the whole system [9]. Kiobayashi and coauthors reported that the starting hydrogen storage capacity of 5 wt. % in the Li-N-H system decreases up to 2 wt. % after 200 cycles tests at 300 °C. This significant reduction of the gravimetric capacity can be, in fact, explained by the loss of nitrogen due to the ammonia release during cycles [9]. For these reasons, many attempts have been made to minimize the ammonia evolution and to drastically improve the poor sorption kinetic performance.

The working temperatures are, in fact, still too high to be practical for a PEM fuel cell, although the activation energies estimated by both Kissinger (54 kJ/mol) and Arrhenius-plots (56 kJ/mol) do not result so high with respect to the observed kinetic constraint [10]. In this regard, when $TiCl_3$ (1 mol. %) is added to the system, almost the 80% of hydrogen is desorbed (5.5 wt. %) within 30 min at 200 °C and without ammonia release [7,11]. $TiCl_3$ acts as a catalyst favoring the transfer of ammonia to lithium hydride and thus improves the hydrogen desorption kinetics of the $LiNH_2$-LiH system. However, the activation energies calculated for the $TiCl_3$-doped system (95 kJ/mol, for 1 mol. % $TiCl_3$) resulted higher than that reported for the un-doped one [10]. In the latter, the small pre-exponential factor has the major effect, therefore it is possible to expect that in the pristine system the reaction occurs through different rate controlling steps. Homogeneous dispersion of Ti(III) species preserves the active surface of reactants and favors the reduction of $LiNH_2$/LiH particles sizes by ball milling [10,11]. This last cited procedure has also an important effect on desorption behavior of the Li-N-H system. As reported by Lu et al. [12], the local Li electronic environment is strongly influenced by mechanical milling, which improves the hydrogen kinetic properties of the $LiNH_2$-LiH composite. Mechanical milling, in fact, is an effective technique to reduce particle size, increase surface area and facilitate the formation of an intimate mixture between the two reagents, $LiNH_2$ and LiH. For example, Shaw and coauthors [13] proved that the hydrogen desorption temperature of Li-N-H in a molar ratio 1:1.1 can

be decreased by high-energy ball milling. In this specific case, the onset dehydrogenation temperature to reach 1 wt. % of released H_2, is reduced from 300 °C in the unmilled material to 50 °C when the powders are subjected to 180 min of mechanical treatment. Furthermore, for the milled powders, no trace of ammonia gas is detected upon desorption. Activation energy seems to be also influenced by ball milling, although completely different values have been reported for the starting system by Shaw et al. with respect to a previous work of Matsumoto et al. [10].

More recently, again Shaw and coauthors [14] showed that milling at liquid nitrogen temperature (−196 °C) is effective in improving the kinetic performance of the powders during hydrogen desorption: the average diffusion rate increases by 450% by milling at liquid nitrogen temperature. Interestingly, the powders upon mechanical treatment at −196 °C show crystallite sizes of 18.3 and 21.5 nm for $LiNH_2$ and LiH, respectively, much higher with respect to the values estimated for the systems milled at room temperature. Therefore, the significant improvement of the desorption kinetics cannot be ascribable to the particle size reduction but, most likely, to the large amount of lattice and surface defect accumulated during milling at low temperature. Another important issue which affects the kinetic properties of this system, is represented by the hydrolysis/oxidation of LiH into LiOH [15]. This reaction sequestrates the active amount of LiH able to convert NH_3 to $LiNH_2$ and H_2 with a reduced hydrogen storage desorption performance. Varin et al. [15,16] studied also the hydrogen storage properties of the $LiNH_2$-LiH systems as a function of the milling time. They measured that the onset DSC (Differential Scanning Calorimetry) peak corresponding to the endothermic desorption step in the 1:1 mixture decreases from 325 °C to 235 °C when the sample is milled 25 h, while in the powders further milled for 100 h the DSC signal is peaked at 245 °C. This is in agreement with the fact that during the milling the Brunauer-Emmett-Teller (BET) specific surface area (SSA) increases monotonically with increase of milling time up to 25 h (16.0, 26.4, 56.0 and 59.6 m^2/g for the system milled at 0, 1, 5 and 25 h). On the other hand, upon 100 h of mechanical treatment, the value of SSA decreases to 45.6 m^2/g, probably due to powders agglomeration induced by the cold-welding process commonly produced in high-energy ball milling.

Another strategy adopted to improve the kinetic and thermodynamic properties of the Li-N-H system is represented by the addition of a second element [16,17] or compounds [16,18–21]. Nayebossadri [17] reported that elemental Si and Al can effectively improve the dehydrogenation rate of the Li-N-H system. In particular, the addition of Si decreases the dehydrogenation end-temperature by 200 °C compared to the pristine material. The destabilization effect can be attributed to the interaction between LiH and Si, which forming the Li_2Si phase increases the concentration of the H^- ions. Varin and coauthors [16], demonstrated that the system $LiNH_2$ + 1.2LiH + graphite (5 wt. %) can absorb reversibly 5 wt. % of H_2 at 325 °C. The inclusion of graphite in the Li-N-H matrix, guarantees an homogeneous heat transfer into the powders and, most important, seems to avoid the undesired hydrolysis/oxidation of LiH normally occurring in the ball milled mixture [16]. Ti- and B-based nitrides additives are also effective to produce a remarkable improvement in the dehydrogenation rate and desorption temperature of the Li-N-H system [19]. High concentration of TiN (35 wt. %) seems to have a significant impact on the kinetic process lowering the activation energy from 163.76 kJ/mol reported for the unmilled material to a promising value of 67.8 kJ/mol.

Structural studies on the Li-N-H system, by using synchrotron facilities as X-ray source, have been performed in order to clarify the reaction mechanism between $LiNH_2$ and LiH [22,23]. David and coauthors, noted that the non-stoichiometric intermediates reported as $Li_{1+x}NH_{2-x}$ species are formed during desorption and absorption of the Li-N-H system, in accordance with the Frenkel defect model [24].

In the Li-N-H system, the poor sorption kinetics in both ab-desorption processes could be ascribable to a reduced Li^+ ion mobility (Li^+ ion conductivity at room temperature is $10^{-8}\ \Omega^{-1}\ cm^{-1}$) [25]. In 2010, Orimo and coauthors [26] have successfully synthesized a new complex hydride $Li_3(NH_2)_2I$ exhibiting lithium fast-ion conductivity of $1 \times 10^{-5}\ \Omega^{-1}\ cm^{-1}$, 1000 times higher than $LiNH_2$. Along this way, Anderson et al. [25,27,28] conducted a systematic study on the effects

of different halides, LiX and MgX_2 (X = Cl, I, Br) on the hydrogen sorption properties of $LiNH_2$ and Li_2NH. The new phases, $Li_4(NH_2)_3Cl$, $Li_3Mg_{0.5}(NH_2)_3Cl$ and $Li_6Mg_{0.5}(NH_2)_6Br$, when heated with LiH are able to release hydrogen more rapidly than pristine $LiNH_2$ and $LiNH_2$ + LiH system, with undetectable NH_3 emission. The general desorption reaction is reported in Equation (3) [25]:

$$Li_{(1+n)}(NH_2)X_n + LiH \rightarrow Li_{(2+n)}(NH)X_n + H_2 \quad (3)$$

Preliminary conductivity analysis on these new amide-halide phases proved that the systems with high ionic conductivity show the quickest hydrogen desorption kinetics during heating [25,29]. More recently, two new halide-amide phases, $Li_7(NH_2)_6Cl$ (SG = R3. a = 9.7367 Å. b = 8.9307 Å) and $Li_6Mg_{0.5}(NH_2)_6Cl$ (SG = R3. a = 9.756 Å. b = 8.9448 Å) have been synthesized and characterized as potential hydrogen storage materials [30]. Both phases, when heated with LiH (1:1), released hydrogen at lower temperatures (150 °C and 200 °C), with no emission of ammonia gas and faster kinetics if compared with the pristine Li-N-H system (220 °C). In addition, rehydrogenation of the dehydrided compounds, in the presence of LiH, is possible under mild conditions of 90 bar H_2 at 300 °C.

Furthermore, as highlighted by Chen et al. [31], another important aspect for improving the hydrogen sorption kinetics is related with the sample morphology and desorption conditions. For example, in the Li_2NH_2Br phase, $LiNH_2$ is confined in the Br cage resulting in less mobility of Li^+ ion. For this reason, the desorption of the Li_2NH_2Br + LiH system follows the NH_3 mediated mechanism although the two components have been intensively ball milled. In other cases, when the $LiNH_2$-type and LiH phases get an intimate mixture, the migrations of Li^+ and H^+ plays a crucial role. Leng et al. [32] showed significant improvements in the desorption properties of the Li-N-H system when mixed with different amounts of $MgCl_2$. From this study emerges that the hydrogen desorption temperatures do not decrease linearly with the increase of $MgCl_2$ amount. Interestingly, for small amount of $MgCl_2$ (1 mol. %), the main hydrogen desorption temperature is reduced to 267 °C, similar to the $TiCl_3$-doped system (265 °C). Increasing the $MgCl_2$ amount up to 4 mol. %, the formation of a solid solution is observed without any improvement in the desorption temperature, while for content of $MgCl_2$ higher than 25 mol. %, a reaction with $LiNH_2$ takes place forming $Mg(NH_2)_2$. Recent works published by Gennari et al. [33,34] introduced $AlCl_3$ as additive and interesting benefits have been reported in terms of ab/desorption rates, cycles stability and hydrogen gravimetric capacity in the Li-N-H system. In a first work [33], it was reported that, for low amount of $AlCl_3$, Al^{3+} is incorporated into the $LiNH_2$ structure which can reversible store 4–5 wt. % of H_2 at 275 °C. Furthermore, the ammonia gas is completely suppressed during desorption reaction. The system was investigated also for increasing amount of $AlCl_3$ (0.03, 0.08 and 0.13 mol) [34]. Interestingly, the dehydrogenation rates of the composite milled with 0.08 mol and 0.13 mol of $AlCl_3$ are three-fold and six-fold faster, respectively, than the pristine system. In particular, upon 5 h of intensive ball-milling of the starting materials $LiNH_2$, LiH and (0.13 mol) $AlCl_3$, a disordered Face Centered Cubic (FCC) solid solution, not yet reported in previous work, is observed. After heating at 300 °C under hydrogen (7 bar), new trigonal and cubic amide-halide (chloride) phases, isostructural with $Li_4(NH_2)_3Cl$ [25], are observed. As reported for the previously cited examples, also in the case of the $AlCl_3$-doped Li-N-H system, the improvement of the hydrogen desorption kinetics is accompanied by a significant reduction of the ammonia release. In this specific case, the preparation of the new cubic and trigonal Li-Al-N-H-Cl phases consisted in ball milling and thermal treatment performed under different atmospheres (argon and hydrogen) of $LiNH_2$ and $AlCl_3$ (0.11 mol) [35]. The whole optimized process is resumed in Figure 2. The desorption reaction of the amide-chloride phases depends on the addition of LiH which completely suppresses the ammonia release and avoids the multi-steps decomposition pathways observed in the post milled $LiNH_2$-$AlCl_3$ composite. The desorbed product, an imide FCC phase (a = 5.172 Å), is re-hydrogenated under moderate temperatures and represents a reversible system. However, despite the progress made to optimize the whole process, the crystal structure of the two active amide-chloride phases, remains unsolved.

The performance, in terms of reversibility and maximum desorption temperatures, of the Li-Al-N-H-Cl system results comparable and in some case better with respect to the most promising doped $LiNH_2$-LiH systems reported in the current literature [18,32,36,37]. For example, after the fourth ab/des cycle the $AlCl_3$-doped composite is able to desorb roughly 92% of the theoretical amount of H_2, significantly higher than the 67% reported for the potassium fluoride KF-doped mixture at the same working temperature (300 °C) [33,36]. A comparison of the maximum desorption temperatures for different doped systems is reported in Figure 3. As emerged, the dopants show a positive effect reducing the desorption temperatures in the $LiNH_2$-LiH system and favoring the release of hydrogen under more moderate conditions. Among them, $AlCl_3$ results to be the most efficient, decreasing the working temperature by 70 °C with respect to the pristine composite.

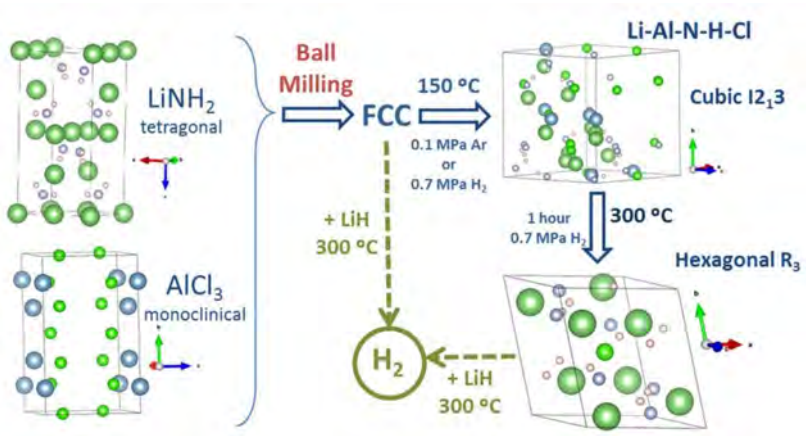

Figure 2. The mechanical treatment of the $LiNH_2$-$AlCI_3$ mixture lead to the formation of a FCC solid solution which, when thermally treated at 150 °C, forms an amide-chloride phase isostructural with a cubic habit (SG $I2_13$). This phase transforms, under H_2 pressure, into the trigonal phase (SG R3) after heating at 300 °C. The addition of LiH to the trigonal phase and FCC solid solution allows to achieve a full and reversible desorption at 300 °C [35].

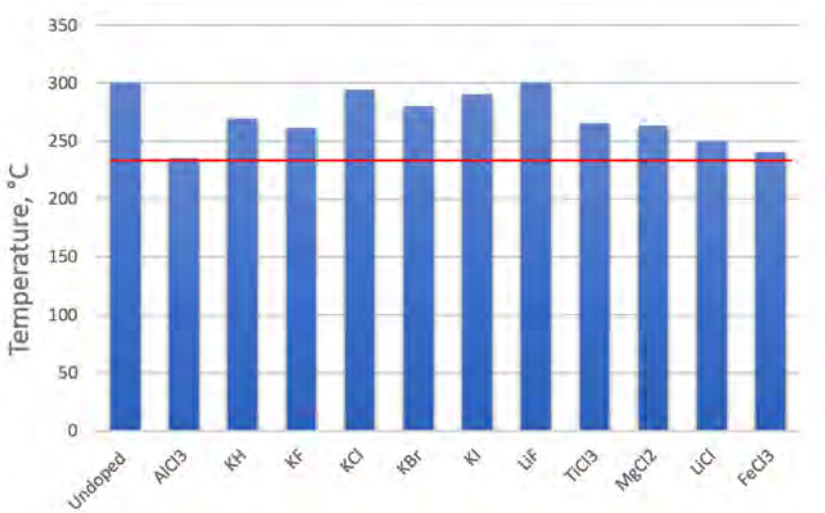

Figure 3. Maximum desorption peak temperatures as a function of different additives on the $LiNH_2$-LiH system. The red line is set on the $AlCl_3$ dopant to highlight its performance.

Gennari et al. [38] also tested the contribution of MgH_2, CaH_2 and TiH_2 in enhancing the kinetic properties of the $LiNH_2$-1.6LiH system. Addition of TiH_2 does not show significant improvement, while for the CaH_2- and MgH_2-based systems positive effects have been reported. For example, the

$LiNH_2$-1.6LiH-0.2CaH_2 systems shows a dehydrogenation rate three time faster at 300 °C than the un-doped materials with about 3.8 wt. % of H_2 stored. Further improvement in terms of working temperature and kinetic rate have been recently reported by Lin and coauthors, by using CeF_4 as efficient catalyst for $LiNH_2$-LiH. This system, when mixed with 10 wt. % of CeF_4 can desorb most of its hydrogen content (~5 wt. %) under milder condition (220 °C) compared with the un-doped mixture. CeF_4 seems to act as a catalyst reducing the activation energy to 114 kJ/mol and suppressing the formation of ammonia gas [39].

The operating temperature of Li-N-H can be reduced by modifying the thermodynamic properties of the system, and, in this context, the substitution of LiH with other metal hydrides represents one of the strategy widely adopted in the recent past [40–46]. Among the most relevant results, it is worth to highlight that the combination of $LiNH_2$ and $LiBH_4$ (2:1) lead to the desorption of a significant amount of hydrogen, around 10 wt. %, at 350 °C. The decomposition of this binary system passes through the formation of a ternary amide, $Li_3BN_2H_8$, which was the object of an intensive study due to the poor reversibility and kinetics constrains [41,42]. For example, Liu and coauthors reported that the addition of $Co(OH)_2$ to the 2$LiNH_2$-$LiBH_4$ mixture significantly improved its hydrogen storage properties. At 200 °C the doped system was able to desorb 9.1 wt. % of hydrogen in only 15 min, while a partial reversibility (1.1 wt. %) was achieved at 350 °C [45]. The activation energy of the doped system was estimated to be 97 kJ/mol, 25% lower with respect to the pristine composite (E_a = 129 kJ/mol). Reversibility under milder conditions (200 °C) was achieved when CaH_2 is added to $LiNH_2$. However, the recharged amount (2.7 wt. % H_2) and the poor kinetic rate (1.1×10^{-4} wt. %/s) represent a strong limitation for this binary system [40].

These new and important results have to be considered in order to improve the hydrogen storage properties of the Li-N-H system, at the moment insufficient for any practical application in the field of the on-board technology. In fact, the thermodynamic data reported in literature show that the equilibrium temperature at H_2 pressure of 1 bar is higher than 200 °C for all the systems analyzed up to now. Such high equilibrium temperature sets this system far from the DoE targets for automotive purposes. For these reasons, further efforts have to be addressed to exploit this system in transportation sector and, in this way, understand the local structure, ion mobility and kinetic constrains to dehydrogenation of the intermediate species $Li_{1+x}NH_{2-x}$ represent the next challenges in this field [47].

3. Li-Mg-N-H System

With respect to the Li-N-H system discussed in the previous section, thermodynamic destabilization can be further achieved by partially replacing Li with Mg, with a significant reduction of the desorption enthalpy down to ca. 40 kJ/mol. The reaction between $LiNH_2$ and MgH_2 (or $Mg(NH_2)_2$ and LiH) for hydrogen storage was reported for the first time in 2004 by five different groups [48–52]. They investigated several factors in the reaction including different ratios between amide and hydride and ab/desorption conditions. Xiong et al. [52] heated lithium amide and magnesium hydride in a 2:1 molar ratio up to 350 °C, and, similar to the Li-N-H system, only hydrogen, without any ammonia, is desorbed. It is found that the hydrogen desorption temperatures are lower than in the $LiNH_2$ + LiH system. From ex-situ powder X-ray Diffraction (XRD) performed on the sample upon heating, new peaks are observed. This new sequence of Bragg reflections does not match with any of the previously identified in the Li-N-H compounds, and it is finally associated with the $Li_2MgN_2H_2$ phase. This ternary imide crystallizes with a cubic lattice (a = 10.035 Å) and its formation is summarized in the following reaction:

$$2LiNH_2 + MgH_2 \rightarrow Li_2Mg(NH)_2 + 2H_2 \quad (4)$$

The solid product of Equation (4) can be re-hydrogenated under 90 bar of H_2 pressure at 180 °C. Upon cycling of the ternary imide, the XRD pattern showed that the products are represented by $Mg(NH_2)_2$ and LiH rather than the original starting materials $LiNH_2$ and MgH_2 (Equation (5)):

$$2LiNH_2 + MgH_2 \rightarrow Li_2Mg(NH)_2 + 2H_2 \leftrightarrow Mg(NH_2)_2 + 2LiH \quad (5)$$

At the same time, Luo [51] also published further work where the absorption and desorption steps of the $2LiNH_2 + MgH_2$ and $LiNH_2$ + LiH systems are compared. The Li-Mg-N-H system starts to desorb hydrogen at lower temperature (100 °C) with respect to the Li-N-H system. Important differences also emerge in the P-C-T curves: the Li-Mg-N-H composite shows a hydrogen equilibrium pressure of 50 bar at 220 °C against the 1 bar of H_2 at 280 °C reported for the Li-N-H mixture. Furthermore, the Li-Mg-N-H sample can be cycled 9 times with no degradation in desorption capacity. Chen et al. [53] investigated in detail the first 4 cycles of the ball-milled $2LiNH_2 + MgH_2$ system. In the first dehydrogenation cycle, the desorption rate is significantly slower than the subsequent three runs, ascribable to the fact that, in the first one, there is an interaction between the $LiNH_2$ and MgH_2. The sorption mechanism, summarized in Figure 4, has been further investigated by Sickafoose et al. [54] In the first step of the isotherm, one hydrogen atom is inserted into the $Li_2MgN_2H_2$ phase, forming $Li_2MgN_2H_3$. The other hydrogen atoms react with $Li_2MgN_2H_3$ in a second step to produce the new species LiH and $Mg(NH_2)_2$.

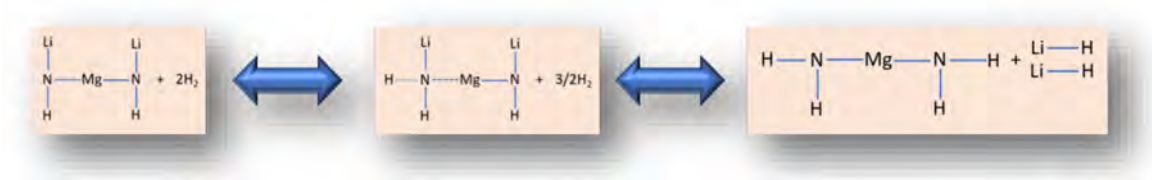

Figure 4. Proposed mechanism in the hydrogen sorption reaction of the $Li_2Mg(NH)_2$ system [54].

Luo et al. [55,56] determined the NH_3 emission in the desorption step of the $2LiNH_2 + MgH_2$ system. The results indicate that the NH_3 concentration is around 180 ppm at 180 °C and 720 ppm at 240 °C, restricting the cycling and then the applicability. Markmaitree et al. [57] compared the reaction kinetics and the NH_3 emission of the $2LiNH_2 + MgH_2$ and $LiNH_2$ + LiH systems. The $2LiNH_2 + MgH_2$ mixture seems to possess a higher activation energy and NH_3 emission than the $LiNH_2$ + LiH mixture. In addition, the samples ball milled for longer time present reduced amount of NH_3 released during the desorption step. This aspect can be explained taking into account the smaller particle size and larger surface area of the produced MgH_2, which favor the interaction with NH_3. When the system is heated up to 210 °C for 5 h, MgNH, $Li_2Mg(NH)_2$ phases and residual $LiNH_2$ and MgH_2 are present in final mixture. On the other hand, after heating for 10 h, $LiNH_2$ and MgNH are completely disappeared, while a small amount of MgH_2 is detected. The main phase is represented by the ternary imide $Li_2Mg(NH)_2$ which suggests that the reaction mechanism involves the decomposition of lithium amide to imide and NH_3 followed by the reaction of MgH_2 with NH_3 as reported in Equation (6):

$$MgH_2 + 2NH_3 \rightarrow Mg(NH_2)_2 + 2H_2. \quad (6)$$

The reaction between MgH_2 and NH_3 takes place with a low rate [58]. The magnesium amide forms and then decomposes to MgNH at a reasonable rate from 250 °C with the release of NH_3 [57]. Further ammonia is produced in the last step, then reacts with residual MgH_2 and the reaction cycle continues. The products from this cycle are MgNH and Li_2NH which could react to form $Li_2Mg(NH)_2$ as suggested in Equation (7):

$$MgNH + Li_2NH \rightarrow Li_2Mg(NH)_2 \quad (7)$$

However, XRD analysis does not support evidence of $Mg(NH_2)_2$ in any step, probably because the reaction reported in Equation (6) proceeds with a slow rate. Furthermore, $Mg(NH_2)_2$ could not be observed by FTIR because of its amorphous nature upon ball milling [59].

Rijssenbeek et al. [60] investigated the hydrogen sorption path of the $2LiNH_2 + MgH_2$ mixture by in situ X-ray diffraction and neutron diffraction. These studies confirm that the dehydrogenated product is a ternary lithium-magnesium imide, $Li_2Mg(NH)_2$, which undergoes two structural transitions from an orthorhombic structure to a primitive cubic structure (β-$Li_2Mg(NH)_2$) at intermediate temperature (350 °C) followed by a face-centered cubic crystal structure (γ-$Li_2Mg(NH)_2$) at high temperature (500 °C). Complete hydrogen absorption is observed for α-$Li_2Mg(NH)_2$ with the formation of $Mg(NH_2)_2$ and LiH. During the dehydrogenation phases of the cycling process, NH_3 is still detected, although in lower amount than the first desorption. It is important to highlight that using $Mg(NH_2)_2$ and LiH as starting materials, the three phases of $Li_2Mg(NH)_2$ can be formed, although α-$Li_2Mg(NH)_2$ is difficult to detect and the β-$Li_2Mg(NH)_2$ phase appears at a lower temperature.

Concerning the experimental thermodynamic properties, Yang et al. [61] estimated a value of ΔH = 41.6 kJ/mol, close to that expected by theoretical calculations [50]. However, although the temperature of hydrogen release is approaching 90 °C, the reaction is kinetically limited. Therefore, to improve the kinetics at temperatures lower than 200 °C, the reaction needed to be catalyzed with suitable dopants or additives. During the last years, many attempts have been made to improve the sorption kinetics of the $2LiNH_2 + MgH_2$ system and, in this context, a large number of papers have been published [62–74]. Luo et al. reported faster absorption kinetics by doping with less than 4 mol. % of KH. In these experiments, the difference in the absorption rates of the doped and undoped systems is particularly noticeable at 180 °C and 115 bar, while it becomes less pronounced at higher temperature and pressure (i.e., 200 °C and 155 bar, respectively) [73]. The studies conducted separately by Yang [75] and Sudik [76] proved that the addition in stoichiometric amount of $LiBH_4$ has a significant impact on the hydrogen storage properties of the Li-Mg-N-H system. Ulmer et al. [71] verified that co-doping with $LiBH_4$ and KH can significantly improve the de/absorption kinetics of the $2LiNH_2 + MgH_2$ system. Interestingly, co-doping with $LiBH_4$ and $ZrCoH_3$ is even more effective: a mixture with composition $2LiNH_2 + 1.1MgH_2$-($0.1LiBH_4$ + 3 mass% $ZrCoH_3$) desorbs 3.2 wt. % under 1 bar H_2 at 180 °C within 100 min and can be re-hydrogenated in only 7 min. The study also demonstrates that this system can be processed efficiently in batches up to 200 g (vibrational mill) and utilized in a tank prototype, showing similar performance to the material processed at lab-scale (planetary mill) [71].

More recently, Goudy et al. [65] showed that RbH added in catalytic amount is significantly better than KH for enhancing the hydrogen sorption properties of the $2LiNH_2 + MgH_2$ system, while the desorption temperature remains almost the same for both dopants. The kinetic findings prove that the RbH-doped system releases hydrogen two and 60 times faster than KH-doped and undoped systems, respectively. In another study, the same authors determine that the desorption rates of the K-, Rb- and Cs-doped $2LiNH_2 + MgH_2$ system increase in the order: undoped < CsH < KH < RbH. Modeling of the kinetic data using a shrinking-core model suggests that the desorption process is diffusion controlled in the first stage of the reaction [66].

To better increase the kinetic reaction and suppress NH_3 emission in efficient manner, Demirocak et al. [64] doped the Li-Mg-N-H mixture with single-walled carbon nanotubes SWCNT/20%Ru catalyst, obtaining an effective elimination of the ammonia gas. Anderson et al. [63], demonstrated that addition of halides ($CaCl_2$ and $CaBr_2$) on the Li-Mg-N-H system can improve the desorption kinetics. In particular, these halides seem to favor the metathesis reaction already during the milling. The lowest dehydrogenation onset temperatures (<100 °C) are achieved in the $2LiNH_2$-MgH_2-0.15CaX (X = Cl_2 and Br_2) system. In particular the $CaBr_2$-doped system presents the lowest desorption onset and peak temperatures (80 °C and 135 °C, respectively) and an activation energy of 78.8 kJ/mol. Combined effect of ball milling and molar ratio $LiNH_2$:MgH_2 on the sorption and structural process were studied by Varin et al. [77,78]. The $LiNH_2 + nMgH_2$ (n = 0.55, 0.6 and 0.7) system is partially converted, by a metathesis reaction promoted by high-energy ball

milling, into $Mg(NH_2)_2$ and LiH. The apparent activation energy of 71.7 kJ/mol is observed for the $LiNH_2$ + 0.7MgH_2 system milled for 25 h, while a further decrease down to 65.0 kJ/mol is obtained when catalyzed by n-Ni composite. The Van't Hoff analysis shows that the equilibrium temperature at 1 bar H_2 is 70.1 °C for this mixture. Additionally, the $LiNH_2$ + 0.7MgH_2 mixture is fully reversible and desorbs/absorbs 3.6 wt. % H_2 at 175 °C.

A mixture of $Mg(NH_2)_2$ and LiH is regarded as an equivalent of the 2$LiNH_2$ + MgH_2 system because of the metathesis reaction between the two hydrides-amides pairs:

$$2LiNH_2 + MgH_2 \rightarrow Mg(NH_2)_2 + 2LiH. \quad (8)$$

The $Mg(NH_2)_2$ + 2LiH system presents some advantages compared to the 2 $LiNH_2$ + MgH_2 composite. For example, as well explained in the previous section, after a cycle of hydrogen desorption/absorption, the 2$LiNH_2$ + MgH_2 mixture becomes a $Mg(NH_2)_2$ + 2LiH system. Considering that this step is accompanied by release of ammonia and kinetic constraints, starting from the $Mg(NH_2)_2$ + 2LiH system is more advisable. One of the first studies on $Mg(NH_2)_2$ + 2LiH was reported by Xiong et al. [79] in 2005. The reactants, ball-milled together for 48 h, upon dehydrogenation at 250 °C release a considerable amount of hydrogen (5.0 wt. %) with the formation of the $Li_2Mg(NH)_2$ phase. The system presents a very appealing reaction enthalpy of 38.9 kJ/mol H_2, but, on the other hand, the activation energy estimated is relatively high (E_a = 102 kJ/mol). Xiong et al. concluded that to decrease the activation energy of this system it is necessary to favor the interaction between H^+ and H^- of the amide and hydride, respectively, or to weaken the Li-N and N-H bonds. Xiong et al. [80] also investigated the effect of molar ratios of $Mg(NH_2)_2$ and LiH, on the desorption properties. The 1:2 mixture presents remarkable differences and better desorption properties with respect to the 1:1 or 1:3 ratios. Furthermore, lower content of LiH favors the desorption of NH_3. These results were also confirmed by other works [81–84]. For example, Hu et al. [82], highlighted that for lower content of LiH, severe ammonia release should be expected, while an excess of LiH affects, in negative, the gravimetric capacity of the system. Liu et al. [85] investigated the effect of sodium compounds on the Li-Mg-N-H system. The hydrogen desorption kinetics of the Na-containing systems are significantly improved and NH_3 emission reduced. The activation energies of the three samples, $Mg(NH_2)_2$ + 2LiH, $Mg(NH_2)_2$ + 1.6LiH + 0.4NaH and 0.8$Mg(NH_2)_2$ + 0.4$NaNH_2$ + 2LiH, are 105.5, 97.7, and 92.5 kJ/mol, respectively. In spite of lower activation energies, the sodium-containing systems possess, as expected, decreased hydrogen gravimetric capacities with respect to the un-doped material. Sudik et al. [86], instead, investigated the effect of $Li_2Mg(NH)_2$ (5 wt. %, 10 wt. % and 15 wt. %) on the sorption properties of the $Mg(NH_2)_2$ + 2LiH systems. The system milled with 10 wt. % $Li_2Mg(NH)_2$ desorbs hydrogen at a 40 °C lower temperature. The desorption curves reveal a two-step hydrogen release as for the un-doped material. Additionally, the activation energy of the $Li_2Mg(NH)_2$-coontaining sample is lowered by 13% from 88.0 kJ/mol to 76.2 kJ/mol. Liu et al. [87] synthesized $Li_2MgN_2H_2$ by annealing a mixture of $Mg(NH_2)_2$-2$LiNH_2$ and investigated its size-dependent hydrogen storage performance. Markedly enhanced kinetics of hydrogen absorption/desorption are achieved with a reduction in the particle and grain size. Janot et al. [88] compared the hydrogen storage performance of the two reactions $Mg(NH_2)_2$ + 2LiH and 2$LiNH_2$ + MgH_2. For the 1:2 MgH_2-$LiNH_2$ system, it evolved ammonia under dynamic vacuum while the ball-milled 1:2 $Mg(NH_2)_2$-LiH mixture desorbs 5.0 wt. % of hydrogen in 25 min at 220 °C and it can be cycled at 200 °C with a total capacity around 4.8 wt. %. Further efforts have been devoted to the kinetic improvement of the $Mg(NH_2)_2$ + 2LiH system by using catalysts or additives [89–94]. Wang et al. [91] proposed graphite-supported Ru nanoparticles as efficient additive in the $Mg(NH_2)_2$ + 2LiH system: after mixing, a considerable enhancement in the ab/dehydrogenation kinetics for more than 10 cycles have been observed. Srivastva et al. [92] proved that the addition of vanadium-based catalysts can catalyze efficiently the desorption reaction of the Li-Mg-N-H system. In particular, the sample mixed with VCl_3 presents a hydrogen desorption temperature lower than the pristine material. This mixture starts to release hydrogen at 50 °C ad its desorption rate is enhanced up to 38%. Similar performance has been obtained in the $Mg(NH_2)$ + 2LH

catalyzed by CaH_2. The desorption starts at temperature of 78 °C and the activation energy estimated for the first dehydrogenation step decreases from a value of 133.8 ± 4.1 kJ/mol in the pristine material to 105.1 ± 3.2 kJ/mol when CaH_2 is added [95].

Significant improvements, in terms of sorption properties and ammonia suppression were achieved by Chen et al. in 2008, either adding $LiBH_4$ or by partially replacing LiH with KH [93,96]. The composite $Mg(NH_2)_2$ + 2LiH + 0.1$LiBH_4$ can desorb and fully re-absorb 5 wt. % of H_2 at temperatures of 140 °C and 100 °C respectively, with a rate three times faster than the undoped material. The system $Mg(NH_2)_2$ + 1.9 LiH + 0.1 KH starts to release hydrogen at temperatures as low as 80 °C. Moreover, complete absorption and desorption can be carried out in equilibrium conditions (Pressure-Composition-Isotherm (PCI) measurements) at 107 °C, revealing a H_2 pressure of 2.5 bar. The hydrogenation can be performed to a considerable extent (ca. 75%) in just 12 min with a hydrogen pressure of 30 bar and a temperature equal to 143 °C: a real breakthrough, considering that for the undoped system 20 h are necessary in order to absorb the same amount of hydrogen. Moreover, differently from the undoped sample, in the KH-containing system the ammonia released was almost undetectable below 200 °C. Several studies tried to identify and characterize the bimetallic intermediates that can be formed from the interaction of KH and $Mg(NH_2)_2$ [97–101]. Interesting results, in terms of hydrogen sorption kinetics, can be achieved using different K-sources, such as KF and KOH, however, the active species seems to be always KH [102–106]. Comparable performance was obtained also with the use of RbF: this was mainly ascribable to the similar structures of $KMgNH_2NH$ and $RbMgNH_2NH$ formed during the dehydrogenation step [107,108]. Interestingly, the addition of both KH and RbH is a simple but effective strategy to further enhance the sorption rate and reversibility of the system [89]. The nominal $Mg(NH_2)_2$ + 2LiH + 0.04KH + 0.04RbH system is able to store 5.2 wt. % of hydrogen reversibly at 130 °C (dehydrogenation)–120 °C (hydrogenation) with a very fast kinetic (43'times faster than pristine material). Furthermore, a noticeable cycling performance has been reported: around of 93% of hydrogen storage capacity remains after more than 50 cycles. Also worth mentioning are the results obtained by using CsH in place of RbH, as single dopant [109] or as co-dopant (with KH) [110] in the $Mg(NH_2)_2$-2LiH system.

In a very recent work, Guo et al. synthesized uniform $Li_2Mg(NH)_2$ nanoparticles embedded into carbon nanofibers, which can ab/desorb efficiently (50 cycles) 2 wt. % of hydrogen at 130 °C. This high performing system exhibits an enthalpy of dehydrogenation of 35.7 kJ/mol H_2, slightly lower if compared with that observed in the bulk system (44.1 kJ/mol H_2). This thermodynamic destabilization was ascribed to both the interaction between the $Li_2Mg(NH)_2$ compound and the carbon matrix and the reduction of the particle size to nanometer scale [111].

4. Li-Mg-N-H-Borohydride Systems

Recently, the Li-Mg-N-H-borohydride system has attracted increasing interest. In fact, the use of borohydrides as additives alters not only the kinetics but also the thermodynamics of Li-Mg-N-H system. Inspired by the richness of the chemistry observed in the binary systems $2LiBH_4$ + MgH_2 [112], $2LiNH_2$ + $LiBH_4$ [41,113] and $2LiNH_2$ + MgH_2 [51,52], a ternary mixture of $2LiNH_2$ + MgH_2 + $LiBH_4$ was investigated by Yang et al. in 2007 [75]. In their following works [114,115], an optimum composition of this ternary system was found to be $6LiNH_2$ + $3MgH_2$ + $LiBH_4$ by combinatorial synthesis and screening techniques. A self-catalyzed reaction mechanism for this ternary composition was proposed: (1) during milling $LiNH_2$ reacts with $LiBH_4$ to form $Li_4BN_3H_{10}$ (Equation (9)); (2) $Li_4BN_3H_{10}$ interacts with MgH_2 producing $Li_2Mg(NH)_2$ (Equation (10)); (3) the formed $Li_2Mg(NH)_2$ functions as seeds for the reaction reported in Equation (5) leading to a general improvement of the hydrogen storage properties [116]. The beneficial effect of "seeding" in improving the dehydrogenation kinetics of Equation (5) has been confirmed by the same group [86]. The drawback of this ternary

system is that the reversible H_2 capacity is a little lower than that of the pristine system. In fact, the maximum reversible H_2 content for the optimum composition is only 3.5 wt. %:

$$3LiNH_2 + LiBH_4 \rightarrow Li_4(BH_4)(NH_2)_3 \quad (9)$$

$$2Li_4(BH_4)(NH_2)_3 + 3MgH_2 \rightarrow 3Li_2Mg(NH)_2 + 2LiBH_4 + 6H_2 \quad (10)$$

The conversion of $LiNH_2$ and MgH_2 into $Mg(NH_2)_2$ and LiH may occur during the dehydrogenation process (Equation (5)). Hu et al. [117], compared the dehydrogenation performance, thermal effects and chemical changes of $1Mg(NH_2)_2 + 2LiH + 1LiBH_4$ and $2LiNH_2 + MgH_2 + LiBH_4$. This investigation showed that MgH_2 and $LiNH_2$ converts to $Mg(NH_2)_2$ and LiH at 120 °C in the presence of $LiBH_4$. Similar results can also be found by changing the ratios of MgH_2 in the $2LiNH_2 + LiBH_4 + x(MgH_2)$ system. During ball milling, MgH_2 reacts with $LiNH_2$ to form $Mg(NH_2)_2$ and LiH together with $Li_4(BH_4)(NH_2)_3$, as reported by Equation (9) [76].

Following these works, Hu et al. [96], introduced $LiBH_4$ as an additive for $Mg(NH_2)_2 + 2LiH$ system. $Mg(NH_2)_2 + 2LiH + 0.1LiBH_4$ shifts its hydrogen desorption onset and maximum peak to lower temperatures, and more than 5 wt. % of H_2 can be reversibly released and stored at 140 and 100 °C, respectively. Furthermore, its theoretical dehydrogenation temperature is 70 °C at 1 bar of hydrogen pressure, which is about 20 °C lower than the pristine system. There are three main reasons for the achieved improvement. Firstly, $LiBH_4$ facilitates the recrystallization of $Mg(NH_2)_2$ after milling, the as formed N-atom matrix in the crystalline of $Mg(NH_2)_2$ shares a similar sublattice structure with the desorption product $Li_2Mg(NH)_2$, similar to the "seeding" effect reported by Yang et al. [86] thus leading to an improvement of dehydrogenation kinetics [118]. Secondly, $Li_4(BH_4)(NH_2)_3$ possess a high Li+ ion conductivity and low melting temperature, which increase the transportation of mass and enlarge the contact between reactants. In addition, being this phase cyclically formed and consumed during the dehydrogenation step, it participates in the capture and release of $LiNH_2$, one dehydrogenation product of $Mg(NH_2)_2 + 2LiH$. Thirdly, $LiBH_4$ alters not only the kinetics but also the thermodynamics of $Mg(NH_2)_2 + 2LiH$ [96,118]. Varying the molar ratio of $Mg(NH_2)_2$, LiH and $LiBH_4$, the optimum molar ratio of 6:9:1 was found [119]. The stabilization of $LiNH_2$, the product of $6Mg(NH_2)_2 + 9LiH$, by adding $LiBH_4$ (Equation (11)) leads to a theoretical dehydrogenation pressure of 1 bar at ca. 64 °C in the $6Mg(NH_2)_2 + 9LiH + LiBH_4$ system:

$$6Mg(NH_2)_2 + 9LiH + LiBH_4 \leftrightarrow 3Li_2Mg_2(NH)_3 + Li_4(BH_4)(NH_2)_3 + 9H_2 \quad (11)$$

To understand the reason for the high dehydrogenation plateau (PCI curves) at the starting stage of dehydrogenation of $6Mg(NH_2)_2 + 9LiH + LiBH_4$, a systematic investigation of the influence of the reactants ratios was carried out [120–122]. Increasing the ratio of $LiBH_4$ in the system $6Mg(NH_2)_2 + 9LiH + xLiBH_4$ to 12, the dehydrogenation enthalpy decreases to 24 kJ/mol H_2 (Figure 5a), allowing to achieve the theoretical equilibrium hydrogen pressure of 1 bar below room temperature. The reason behind this interesting property is the role played by the addition of high amount of $LiBH_4$ which strongly influences the dehydrogenation pathway. PCI curves of $6Mg(NH_2)_2 + 9LiH + 12LiBH_4$ show the existence of two plateaus, one at high pressure and another having a sloppy appearance (Figure 5b). The overall dehydrogenation reaction for the PCI process has been proposed to be as follows: firstly, dehydrogenation occurs from the reaction between $Mg(NH_2)_2$ and LiH, forming MgNH, $LiNH_2$ and H_2; then the as-formed $LiNH_2$ surrounded by $LiBH_4$ produces a mixture of $LiNH_2$-$2LiBH_4$ (Equation (12)). This is the reason for the presence of the high-pressure plateau in the PCI curves (Figure 5b). Secondly, $LiNH_2$ reacts with LiH to form H_2 and Li_2NH with the help of $LiBH_4$, leading to the H_2 desorption in the sloppy pressure region (Equation (13)) [122]:

$$2Mg(NH_2)_2\ (s) + 2LiH\ (s) + 4LiBH_4\ (s) \leftrightarrow 2MgNH\ (s) + 2[LiNH_2 + 2LiBH_4]\ (l) + 2H_2\ (g) \quad (12)$$

$$2MgNH\ (s) + 2[LiNH_2 + 2LiBH_4]\ (l) + LiH\ (s) \leftrightarrow 2MgNH\ (s) + 2[(Li_2NH + 2LiBH_4) - (LiNH_2 + 2LiBH_4)]\ (l) + H_2\ (g) \quad (13)$$

The volumetric characterization of this system shows a significant release of hydrogen around 98 °C, close to the operating temperature of PEM fuel cell. However, very fast kinetics, suitable for practical applications, are possible only at 143 °C.

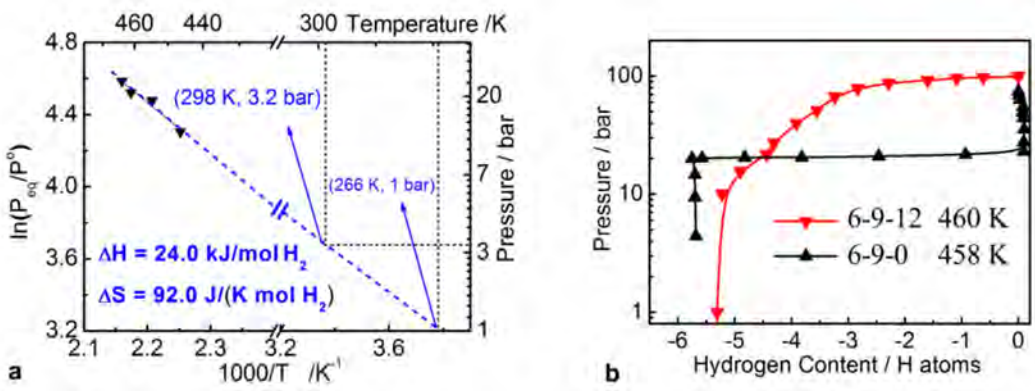

Figure 5. (**a**) van't Hoff plot of $6Mg(NH_2)_2$ + 9LiH + $12LiBH_4$; (**b**) PCI curves for $6Mg(NH_2)_2$ + 9LiH + $12LiBH_4$ and $6Mg(NH_2)_2$ + 9LiH at ca. 460 K [122].

Similarly to the reaction between $LiNH_2$ and $LiBH_4$, Li_2NH can also react with $LiBH_4$ forming several different compounds [123–125]. Interestingly, these compounds have extremely appealing Li^+ ion conductivity. The ionic conductivity of such compounds is a key factor in improving the kinetic properties of the $Mg(NH_2)_2$ + LiH system [126,127]. Examples of such compounds in the $Mg(NH_2)_2$ + LiH + $xLiBH_4$ system are $Li_2(BH_4)(NH_2)$, $Li_3(BH_4)(NH_2)_2$, and $Li_4(BH_4)(NH_2)_3$. The Li^+ conductivity of $Li_2(BH_4)(NH_2)$ is around 2×10^{-4} S cm^{-1} at room temperature (RT). Upon heating to 105 °C, its conductivity reaches to 6×10^{-2} S cm^{-1}. $Li_4(BH_4)(NH_2)_3$ also possesses a high Li^+ conductivity of 2×10^{-4} S cm^{-1} and 1×10^{-3} S cm^{-1} at RT and 100 °C, respectively [128].

Recently, various transition metal salts [129–135] were tested as additives to further improve the hydrogen properties of the $LiBH_4$-doped Li-Mg-N-H system. For example, Li_3N and YCl_3 have been used as co-additives for $6Mg(NH_2)_2$ + 9LiH + $xLiBH_4$. The co-additives improve the hydrogen storage capacity and the de/absorption kinetics. 4.2 wt. % of hydrogen was charged in only 8 min under isothermal conditions at 180 °C and 85 bar of hydrogen pressure. Furthermore, by increasing the H_2 pressure above 185 bars, the absorption process can be performed under milder temperature conditions below 90 °C. These hydrogenation capacity and absorption kinetics can be maintained constant for more than 10 cycles [135]. The reaction mechanism depicted in Figure 6, proposed for the hydrogenation step, reveals that hydrogen is firstly dissociated by the action of the additive and then interacts with the ternary imide $Li_2Mg(NH)_2$ forming the binary system $Mg(NH_2)_2$-LiH. The diffusion of hydrogen and the mass transfer is ruled by the liquid matrix $Li_4(BH_4)(NH_2)_3$.

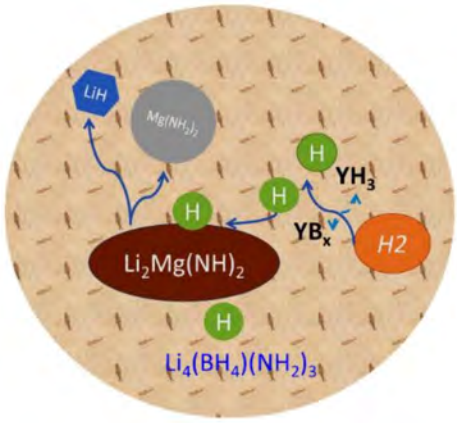

Figure 6. Scheme of the reaction mechanism proposed for the re-hydrogenation step in the co-additive $6Mg(NH_2)_2$ + 9LiH + $xLiBH_4$ systems [128].

The effect of some nanoadditives such as Ni, Co, Fe, Cu, and Mn have been investigated by Srinivasan et al. [129] for the $2LiNH_2$ + $1.1MgH_2$ + $0.1LiBH_4$ system, previously introduced in the Section 3. As the result of this investigation, it was found that some of these additives (Co, Ni) reduce the de-hydrogenation temperature of more than 75 °C; some others (Cu, Fe) increase significantly the de-hydrogenation rate.

However, one of the most efficient additives for the $2LiNH_2$+$1.1MgH_2$+$0.1LiBH_4$ system still remains $ZrCoH_3$ [130]. The addition of 3 wt. % of $ZrCoH_3$ to this system leads to absorb 5.3 wt. % of H_2 under 70 bar of H_2 pressure in 10 min and desorb 3.8 wt. % of H_2 under 1 bar H_2 pressure in 60 min at 150 °C. X-ray absorption fine structure (XAFS) study suggests that the chemical environment of both Zr and Co atoms and the crystal parameters of $ZrCoH_3$ remain unchanged during de/re-hydrogenation processes. These results point out to the fact that $ZrCoH_3$ works as a catalyst in this ternary composition [131]. $2LiNH_2$ + $1.1MgH_2$ + $0.1LiBH_4$-3 wt. %$ZrCoH_3$ has been considered as one of the most promising materials for possible real scale applications owing to its excellent hydrogen storage properties [136–138]. A prototype tank to feed a 1 kW HT-PEM stack for an Auxiliary Power Unit (APU), was built using this ternary system as storage material. The gravimetric capacity of this tank was roughly 2.1 wt. %, fully reversible at the temperature range of 160–180 °C [138].

Other borohydrides such as $Mg(BH_4)_2$ [139–141] and $Ca(BH_4)_2$ [142] were also added to the system, and similar effects to that of $LiBH_4$ were observed. For example, the $Mg(NH_2)_2$ + 2LiH + $0.1Mg(BH_4)_2$ sample can reversibly de/re-hydrogenate ~4.5 wt. % of H_2 at 140 and 120 °C. $Mg(BH_4)_2$ and LiH convert to $LiBH_4$ and MgH_2 during ball milling, subsequently, the as formed MgH_2 reacts with $Mg(NH_2)_2$ to form MgNH. Upon heating, $LiBH_4$ support the recrystallization of $Mg(NH_2)_2$ and reacts with $LiNH_2$ to form $Li_4(BH_4)(NH_2)_3$. Meanwhile, MgNH may act as a seeding agent for $Li_2Mg(NH)_2$ leading to a fast dehydrogenation of $Mg(NH_2)_2$ and LiH as the consequence of the structural similarity. Thus, the as formed $LiBH_4$ and MgNH synergistically influence the hydrogen storage performances of the $Mg(NH_2)_2$ + 2LiH system [140]. Recently, $Li_4(BH_4)(NH_2)_3$ has also been tested as an additive to alter the hydrogen storage properties of the Li-Mg-N-H system due to its low melting point and fast Li^+ ion conductivity [143–146].

5. Ternary Transition Metal Amide-Hydride System

Various amide-hydride systems with different kinetics and thermodynamics have been developed by the combination and/or replacement of several amides and/or hydrides. Meanwhile, doping with transition metal/salt such as Sc, Ti, V, Ta, Ni et al. has demonstrated to be an effective way to improve the hydrogen storage properties of amide-hydride system. The hydrogen sorption properties of $LiNH_2$

+ LiH can be significantly improved by doping it with nanosized Ti-based additives. In fact, this system can desorb roughly 5.5 wt. % H_2 within a temperature range of 150 to 250 °C.

Considering the advantages achievable by following both ways of improving the hydrogen storage performance, recently we introduced several ternary alkali metal transition metal amides as hydrogen storage materials after mixing them with LiH. For some of the investigated systems, outstanding absorption kinetics have been observed. As an example, the product of the decomposition of $K_2[Zn(NH_2)_4]$ + 8LiH can be fully hydrogenated within 30 s, as reported in Figure 7, at 230 °C and 50 bar of H_2 [147]. Similar phenomenon was also observed in $K_2[Mn(NH_2)_4]$ + 8LiH under the same temperature and hydrogen pressure conditions [148].

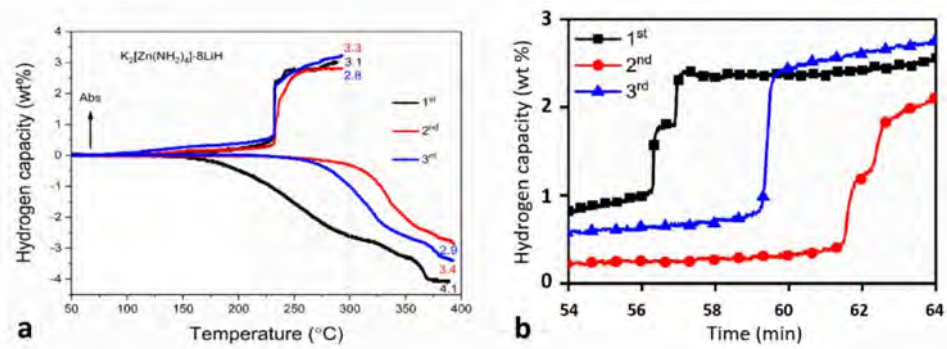

Figure 7. Volumetric desorption and absorption cycles of the $K_2[Zn(NH_2)_4]$ + 8LiH system vs. temperature (**a**) and time (**b**). The desorption step has been performed from room temperature to 400 °C (3 °C/min) under static vacuum while the absorption from room temperature to 300 °C (3 °C/min) under 50 bar H_2. [147].

The details of the reaction pathway of $K_2[Zn(NH_2)_4]$ + 8LiH system were investigated by means of in situ X-ray diffraction studies (Figure 8) [149]. This study showed that $K_2[Zn(NH_2)_4]$ + 8LiH converts to $4LiNH_2$ + 4LiH + K_2ZnH_4 during milling; upon heating, $4LiNH_2$ + 4LiH + K_2ZnH_4 releases H_2 in multiple steps. The final dehydrogenation products are KH, $LiZn_{13}$, and Li_2NH. During absorption, KH reacts with $LiZn_{13}$ under 50 bar of H_2 to form K_3ZnH_5. This phase most likely is the key to enhance the re-hydrogenation process; thanks to the existence of K_3ZnH_5, the absorption reaction takes place in only 30 s at ca. 220 °C [149]. Inspired by these works, a large variety of ternary metal transition amides can be produced opening new perspectives for the development of systems which can ab/desorbs hydrogen at lower temperatures more suitable for practical applications.

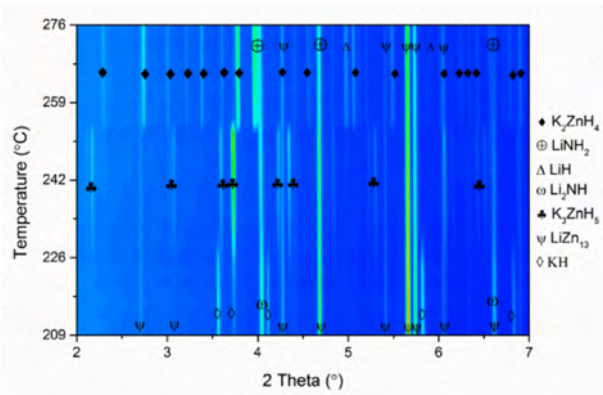

Figure 8. Re-hydrogenation contour plot of the $K_2[Zn(NH_2)_4]$ + 8LiH composite at the temperature range between 209 and 276 °C (heating rate of 2 °C/min, λ = 0.20775 Å) [149].

6. Sodium-Based Composites

In the last 10 years, the ever-increasing cost of lithium on a worldwide scale has encouraged the search for lithium-free metal amides systems with high-performing properties for on-board applications, which can replace the most expensive Li-based amides. $NaNH_2$ and its composites, in particular, have attracted a lot of attentions because its considerable high amount of hydrogen, low cost and interesting thermodynamic properties [150–154].

Due to its high catalytic activity in the decomposition of NH_3, pure sodium amide, has been considered as potential material also for other applications different from solid-state hydrogen storage. In this context, its decomposition path has been topic of debate. Recently, two different decomposition paths have been presented. Jain et al. [151], proposed that $NaNH_2$, after melting at 200 °C, decomposes to sodium, ammonia and nitrogen (>400 °C), without passing for its corresponding nitride and/or imide phase as, on the other hand, shown by $LiNH_2$ and $Mg(NH_2)_2$. Recently, different results have been obtained by Miyaoka and coauthors, where the thermal decomposition of sodium amide was studied under different experimental conditions [154]. From this specific study emerged that the decomposition reaction products depend on the pressure conditions. The authors discovered a new intermediate, an imide-like phase with a cubic structure, which decomposes to sodium, at 400 °C, under vacuum, while, for the closed system, the partial pressure of hydrogen promotes the formation of sodium hydride [154].

A significant reduction of the hydrogen desorption temperatures, has been successfully obtained for composite systems. For example, Pecharsky et al. [153] reported that the $2NaNH_2 + 3MgH_2$ system released hydrogen in the temperature range of 130–400 °C (vs. 186 °C–400 °C for $2LiNH_2 + 3MgH_2$) following the Equation (14):

$$2NaNH_2 + 3MgH_2 \rightarrow Mg_3N_2 + 2NaH + H_2 \quad (14)$$

A total release of 5.1 H_2 wt. % was finally achieved at 400 °C. The decomposition path summarized in Equation (14) proceeds with a series of competitive solid-state process including the formation of $Mg(NH_2)_2$ at low temperature (>140 °C), which suggests that a metathesis reaction occurred. Only 2.1 wt. % of hydrogen could be re-absorbed at 395 °C under 190 bars of hydrogen, probably because, at this high temperature, NaH is liquid and/or decomposes to Na. However, any absorption was achieved at lower temperatures. New insights on the desorption pathway of $NaNH_2/MgH_2$ were obtained by Sheppard and collaborators [152]. 3.3 wt. % of hydrogen was in fact desorbed between 70 and 335 °C in the equimolar milled system with the formation of two new magnesium-containing imide and nitride phases during the dehydrogenation. Despite the lower desorption temperature with respect the 3:2 system, the kinetic desorption remains a not yet solved limitation for this mixture even after the addition of catalysts such as $TiCl_3$.

Effect of high-energy ball milling on the $NaNH_2/MgH_2$ systems with different stoichiometry, 2:1 and 2:3, have also been evaluated [155–157]. The mechanically activated metathesis reaction occurred for the 2:1 system, ball milled for a prolonged milling time. Without releasing of hydrogen gas. Conversely to the thermally activated process, which exhibits solid intermediates, only the formation of $Mg(NH_2)_2$ and NaH phases were observed upon the extended mechanical treatment (50 h). This represented a valid strategy to prepare the $Mg(NH_2)_2$-NaH system in nanostructured conditions. However, in the same work, it emerged that the desorption properties cannot be interesting for practical applications [156]. This evidence was also confirmed by a previous work, published by Chen et al. devoted to the study of the Mg-Na-N-H system [158]. $Mg(NH_2)_2$ was mixed with different amounts of NaH and the hydrogen storage properties tested. Working temperatures lower than 200 °C were observed but only 2.17 wt. % of hydrogen could be reversibly desorbed, which implies a scarce interest from a practical applications point of view.

One of the most important benefit recognized to the addition of metal hydrides to sodium amide, is represented by the ammonia suppression during the thermal decomposition step, as reported by

Jain et al. [159] In this work, NaH has been shown to efficiently suppress the emission of ammonia gas when added to $NaNH_2$. Furthermore, a clear picture of the mechanism involved in this process has been reported for an extended number of amide hydride systems: the dehydrogenation process occurred with the formation of double-cation amides, which decrease the hydrogen desorption temperatures (except for the CaH_2-containing system) [159].

A further way to destabilize $NaNH_2$ is represented by the addition of complex hydrides, such as $NaBH_4$, $Ca(BH_4)_2$ and $Mg(BH_4)_2$ in stochiometric amount [150,158,160–163]. For example, the starting reagents $NaNH_2$-$NaBH_4$ (2:1) when subjected to intensive ball milling, react producing $Na_3(NH_2)_2BH_4$. This new phase desorbed hydrogen (6.85 wt. %) gas forming Na_3BN_2 [162]. The desorption path is characterized by two main steps: the first in the temperature range 70–170 °C, while the second one between 190–420 °C. At higher temperatures, Na_3BN_2 decomposes to Na. The activation energy of this system was estimated to be 159.6 kJ/mol, and it can be significantly reduced to 70 kJ/mol by the addition of Co-B catalyst [163]. A comparable kinetic enhancement was also reached for the un-doped 2:1 system prepared by liquid phase ball milling (E_a = 76.4 kJ/mol) instead of the classical dry milling, paving the way for the exploration of a new efficient synthetic route for this kind of composites [161]. Synergetic effect of the liquid phase ball milling preparation and the addition of Co-Ni-B dopant, contributed to significantly improve the kinetic performance of the dehydrogenation step further lowering the activation energy to 68.2 kJ/mol and the thermodynamic property of the system. In fact, 5.05 wt. % of hydrogen was successfully desorbed at temperature below 200 °C [163].

Concerning the addition of $Mg(BH_4)_2$ and $Ca(BH_4)_2$, a very recent and detailed structural investigation was performed for different compositions [160]. Both the systems desorbed by the emission of undesired ammonia gas at low temperature while the formation of $NaBH_4$ occurred through a metathesis reaction between $NaNH_2$ and $M(BH_4)_2$ (M = Mg, Ca). Hydrogen gas evolution started only at temperature higher than 350 °C for the 1:2 system and above 450 °C for the equimolar 1:1 composites, making these systems not properly suitable for on-board applications.

Finally, different studies have also been focused on the opportunity to improve the hydrogen storage properties of $NaNH_2$ by combining it with $LiAlH_4$ as effectively occurred for $LiNH_2$ [164–167]. In this context, Xiong et al. proved that during ball milling a solid-state interaction between $NaNH_2$ and $LiAlH_4$ took place, leading to the formation of the tetramide $Li_3Na(NH_2)_4$ which seems to favor the desorption at lower temperatures [166]. Recently, Jensen and coauthors synthesized, by high-energy ball milling the lithium sodium tetramide and corroborated its key role together with $LiNa_2(NH_2)_3$, in the destabilization of different sodium-based systems [165]. For example, $LiNH_2$-NaH and $NaNH_2$-LiH desorbed 0.9 wt. % of hydrogen from 180 to 340 °C with a faster kinetic if compared with the most explored $LiNH_2$ + LiH system. Unfortunately, as emerged from in situ synchrotron X-ray powder diffraction (XRPD) studies, imides and nitrides cannot be formed under moderate temperatures, which implies the irreversibility of these systems.

7. Concluding Remarks

The technological challenges connected with the exploitation of solid materials for storing efficiently hydrogen are primary sources of interest, and the opportunity to use metal amides-based composites in this specific area captures the attention of an increasing number of scientists. From the overview offered in Section 2, it is clear that the Li-N-H system, despite of the encouraging results recently obtained, possess several limitations, in particular from the thermodynamic point of view, which are in part mitigated when Li is partially replaced by Mg, forming the Li-Mg-N-H system. The latter, in fact, shows more suitable thermodynamic properties and superior kinetics when compared with the first one. To get light on the promising properties of these systems, the thermodynamic and kinetics features of the most appealing mixtures, experimentally achieved, have been summarized in Table 1.

Table 1. Thermodynamic and kinetic data of some Li-Mg-N-H systems.

Composition	ΔH kJ/(mol H_2)	ΔS J/(mol K)	E_a kJ/mol	Hydrogen Content—wt. % (Desorption Working Temperature and Time)	Ref.
$2LiNH_2 + MgH_2$	65.0 65.8	-	119.0 119.0	2.8 (210 °C, 250 min) -	[66] [65]
$1.9LiNH_2 + 1.1MgH_2 + 0.1KH$	42.0	-	87.0	5.4 (210 °C, 250 min) 5.0 (210 °C, 50 min)	[65]
$1.9LiNH_2 + 1.1MgH_2 + 0.1RbH$	42.7	-	86.8	5.5 (210 °C, 50 min)	[65]
$1.9LiNH_2 + 1.1MgH_2 + 0.1CsH$	45.7	-	109.1	5.0 (210 °C, 100 min) 4.4 (210 °C, 50 min)	[66]
$2LiNH_2 + MgH_2 + 0.1LiBH_4$	-	-	156	2.5 (180 °C, 180 min)	[145]
$2LiNH_2 + MgH_2 + 0.1LiBH_4$ + 4 wt. % $ZrFe_2$	54.0	159.6	135	4 (180 °C, 180 min)	[145]
$2LiNH_2 + MgH_2 + 0.1LiBH_4$ + 3 wt. % $ZrCoH_3$	45.0	124.0	131.8 79.9	4.1 (150 °C, 450 min) 4.5 (150 °C, 350 min)	[131,136] [134]
$Mg(NH_2)_2 + 2LiH$	38.9 41.6	112.0	102.0 112.2	5.0 (200 °C) 2.6 (140 °C, 400 min)	[79] [140]
$6Mg(NH_2)_2 + 9LiH$	40.1	113.3	-	2.8 (146 °C, 500 min) 4.4 (81 °C) *	[119]
$6Mg(NH_2)_2 + 9LiH + 3/2LiI$	33.3	99.9	-	2.4 (146 °C, 500 min) 3.0 (60 °C) *	[119]
$6Mg(NH_2)_2 + 9LiH + 3LiBr$	31.9	99.5	-	1.8 (146 °C, 500 min) 2.7 (48 °C) *	[119]
$6Mg(NH_2)_2 + 9LiH + LiBH_4$	35.8	106.2	-	4.0 (146 °C, 500 min) 4.0 (174 °C-15 cycles) 4.2 (64 °C) *	[119,135]
$6Mg(NH_2)_2 + 9LiH + 3LiBH_4$	-	-	109.0	3.8 (143 °C, 220 min)	[121]
$6Mg(NH_2)_2 + 9LiH + 6LiBH_4$	-	-	86.0	3.3 (143 °C, 220 min)	[121]
$6Mg(NH_2)_2 + 9LiH + 12LiBH_4$	24	92	76.0	2.6 (98 °C, 140 h) 2.6 (108 °C, 40 h) 2.6 (143 °C, 8 h) 2.7 (RT) *	[121,122]
$6Mg(NH_2)_2 + 9LiH + LiBH_4$ + 2 wt. % YCl_3	-	-	130.0	1.9 (140 °C, 800 min)	[135]
$6Mg(NH_2)_2 + 9LiH + LiBH_4$+5 wt. % Li_3N	-	-	134.0	1.9 (140 °C, 800 min)	[135]
$6Mg(NH_2)_2 + 9LiH + LiBH_4$ + 2 wt. % YCl_3 + 5 wt. % Li_3N	-	-	128.0	2.1 (140 °C, 800 min)	[135]
$Mg(NH_2)_2 + 2LiH + 0.1LiBH_4$	36.5	105.6	-	4.3 (140 °C, 400 min)	[96]
$Mg(NH_2)_2 + 2LiH + 0.2LiBH_4$	38.5	-	101.4	3.7 (140 °C, 400 min)	[140]
$Mg(NH_2)_2 + 2LiH + 0.1Mg(BH_4)_2$	36.7	-	99.7	4.1 (140 °C, 400 min)	[140]
$Mg(NH_2)_2 + 2LiH + 0.2MgNH$	-	-	105.5	3.1 (140 °C, 400 min)	[140]
$Mg(NH_2)_2 + 1.9LiH + 0.1KH$	42.0	-	-	4.8 (163 °C, 50 min)	[93]
Mg(NH2)2 + 2LiH + 0.08KF	39.4	-	-	4.3 (150 °C, 150 min)	[104]
$Mg(NH_2)_2 + 2LiH + 0.08RbF$	39.3	-	-	3.6 (130 °C, 350 min)	[107]
$Mg(NH_2)_2 + 2LiH + 0.04KH + 0.04RbH$	38.0	-	-	3.8 (130 °C, 350 min)	[89]
$Li_2Mg(NH)_2$@CNFs	35.7	100.2		2.0 (130 °C, 50 min)	[111]

* theoretical dehydrogenation temperature over 0.1 MPa equilibrium hydrogen pressure.

Depending on the dopant, the $2LiNH_2 + MgH_2$ system shows different behaviors. In comparison to the un-doped material, the addition of additives based on KH; RbH and CsH, (Figure 9), lead to significant thermodynamic and kinetic improvements. The introduction of $LiBH_4$ contributes to decrease the temperature of hydrogen release from 210 °C to 180 °C, however, the gravimetric capacity of the system is affected. An important enhancement is produced when this composite is doped with $ZrFe_2$ and $ZrCoH_3$, as clearly emerged by the bars in Figure 10. The system containing $ZrCoH_3$ has been extensively investigated and, up to day, among the metal amide-based family, it is probably the only system tested under near practical conditions [137].

Interestingly, the working temperature can be further decreased inverting the system cations, i.e., $Mg(NH_2)_2$-LiH. This composite presents several advantages such as reduced or almost suppressed ammonia emissions, working temperatures of about 150 °C and good gravimetric capacity if compared with the previous composites (Figure 10). For this system, the enthalpy is reduced from ~50 kJ/mol H_2 of the $LiNH_2/MgH_2$-based mixtures to ~40 kJ/mol H_2. However, as also evidenced in Table 1, the data concerning the activation energy of the dehydrogenation process are quite scarce and more efforts have to be made to obtain a more detailed picture of this system.

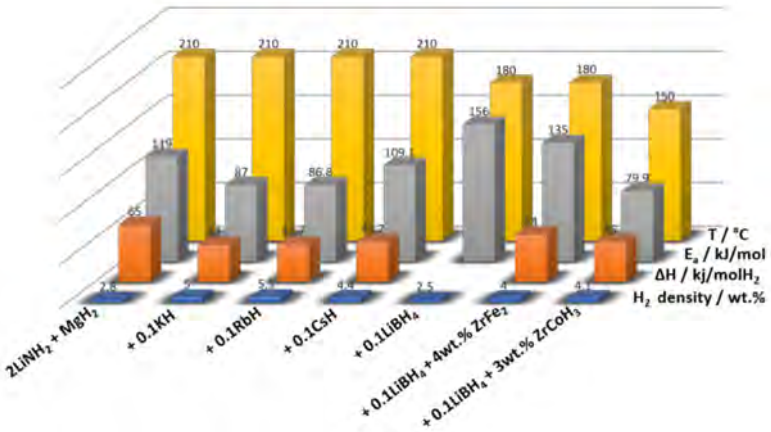

Figure 9. Experimental thermodynamic and kinetic data for the un-doped and doped $2LiNH_2$ + MgH_2 systems.

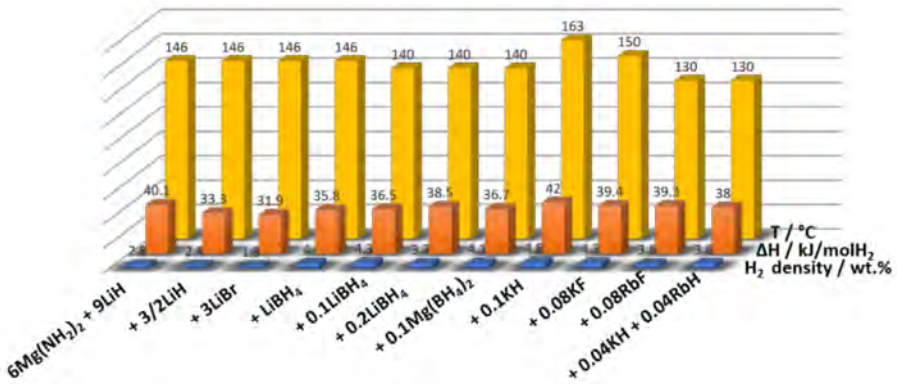

Figure 10. Experimental thermodynamic and kinetic data for the un-doped and doped $Mg(NH_2)_2$ + 2LiH systems.

In order to better discriminate among the most appealing systems which approach to the targets fixed by DoE, two main parameters, gravimetric density and working temperature properties have been selected and depicted in Figure 11 for several materials. Other systems not discussed in this review, such as NH_2NH_2, $LiBH_4 * N_2H_4$, metal borohydrides, etc., have been also included in the graph, for comparison purpose. Form these data it is possible to evince that, by now, there is no amides-based system which can completely fits the specific targets fixed by DoE for 2020 (olivine panel in Figure 11). However, it is important to highlight the important progresses made in the last years in term of effective working temperature. In particular, the ternary system $Mg(NH_2)_2$ + LiH + $LiBH_4$ shows a working temperature close to the desired room temperature. $LiBH_4$ is proved to have an extraordinary effect in tuning the thermodynamic properties of the Li-Mg-N-H system. Likewise, nanoparticles of $Li_2Mg(NH)_2$ encapsulated into carbon nanofiber matrix possess suitable temperature to be candidate as promising material for practical application. However, the hydrogen release under these operative conditions is not enough to satisfy the expected requirement.

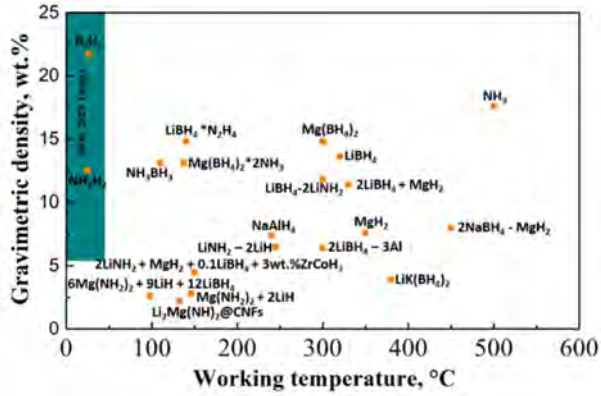

Figure 11. Working gravimetric density and temperatures of some representative materials for hydrogen storage applications.

Furthermore, despite the reaction enthalpy of 24 and 35.7 kJ/mol H_2, results quite satisfactory, both systems are kinetically hindered. In fact, in the ternary composites desorbs reversibly 2.8 wt. % of hydrogen below 100 °C only after 140 h. The encapsulated system can reversibly release similar amount of hydrogen with faster kinetic (50 min) but under higher temperature (130 °C). For this reason, at the moment, kinetic improvement represents the first objective to be accomplished for these systems and many efforts have to be addressed in this direction as future perspective. In this context, solid-state catalysts, using K-and Rb-based additives, or $ZrCoH_3$, can represent a valid strategy, together with a suitable preparation technique, for reaching the expected results for both these systems.

Another challenge is represented by scaling-up the production of the specific systems. This implies to approach two main important aspects: (i) the preparation techniques and (ii) cost of materials. If $Li_2Mg(NH)_2$@CNFs presents a restricted number of solid reagents involved in its preparation, which reduces the whole cost of production, the soft chemistry approach used in this synthesis is, of course, less practicable for producing large amounts of product with respect to the traditional ball milling. Likewise, the cost issue of the starting materials has to be taken in consideration. The commercial prices of the involved materials are reported in Table 2. The actual costs of reagents represent a further barrier for a rapid commercialization of these systems. However, a valid chance, in prospective, can be represented by using cheap raw materials obtained from Mg and Li industrial wastes, which can allow to halve the production cost of several amides.

Table 2. Commercial prices of materials involved in the preparation of the metal amides-based composites.

Materials	$LiNH_2$	LiH	MgH_2	$LiBH_4$
Purity (%)	95 (Alfa Aesar) 95	97 (Alfa Aesar)	95% (Albemarle)	95 (Acros Organics)
Price (€/kg)	348	483	600	7980

Author Contributions: Antonio Santoru, Hujun Cao, Sebastiano Garroni and Claudio Pistidda realized the structure design of the manuscript and the recovering of the data. Chiara Milanese, Fabiana Gennari, Thomas Klassen and Martin Dornheim contributed to the writing and revision of the review.

Acknowledgments: The authors acknowledge the funding from European Marie Curie Actions under ECOSTORE grant agreement No. 607040.

Conflicts of Interest: The authors declare no conflict of interest.

References

1. Chen, P.; Xiong, Z.; Luo, J.; Lin, J.; Tan, K.L. Interaction of hydrogen with metal nitrides and imides. *Nature* **2002**, *420*, 302–304. [CrossRef] [PubMed]

2. Chen, P.; Zhu, M. Recent progress in hydrogen storage. *Mater. Today* **2008**, *11*, 36–43. [CrossRef]
3. Pinkerton, F. Decomposition kinetics of lithium amide for hydrogen storage materials. *J. Alloys Compd.* **2005**, *400*, 76–82. [CrossRef]
4. Chen, P.; Xiong, Z.; Luo, J.; Lin, J.; Tan, K.L. Interaction between lithium amide and lithium hydride. *J. Phys. Chem. B* **2003**, *107*, 10967–10970. [CrossRef]
5. Ichikawa, T.; Hanada, N.; Isobe, S.; Leng, H.; Fujii, H. Mechanism of novel reaction from $LiNH_2$ and LiH to Li_2NH and H_2 as a promising hydrogen storage system. *J. Phys. Chem. B* **2004**, *108*, 7887–7892. [CrossRef]
6. Hino, S.; Ichikawa, T.; Ogita, N.; Udagawa, M.; Fujii, H. Quantitative estimation of NH_3 partial pressure in H_2 desorbed from the Li-N-H system by Raman spectroscopy. *Chem. Commun.* **2005**, 3038–3040. [CrossRef] [PubMed]
7. Ichikawa, T.; Isobe, S.; Hanada, N.; Fujii, H. Lithium nitride for reversible hydrogen storage. *J. Alloys Compd.* **2004**, *365*, 271–276. [CrossRef]
8. Meisner, G.P.; Pinkerton, F.E.; Meyer, M.S.; Balogh, M.P.; Kundrat, M.D. Study of the lithium–nitrogen–hydrogen system. *J. Alloys Compd.* **2005**, *404–406*, 24–26. [CrossRef]
9. Ikeda, S.; Kuriyama, N.; Kiyobayashi, T. Simultaneous determination of ammonia emission and hydrogen capacity variation during the cyclic testing for $LiNH_2$–LiH hydrogen storage system. *Int. J. Hydrogen Energy* **2008**, *33*, 6201–6204. [CrossRef]
10. Matsumoto, M.; Haga, T.; Kawai, Y.; Kojima, Y. Hydrogen desorption reactions of Li–N–H hydrogen storage system: Estimation of activation free energy. *J. Alloys Compd.* **2007**, *439*, 358–362. [CrossRef]
11. Ichikawa, T.; Hanada, N.; Isobe, S.; Leng, H.; Fujii, H. Hydrogen storage properties in Ti catalyzed Li–N–H system. *J. Alloys Compd.* **2005**, *404*, 435–438. [CrossRef]
12. Lu, C.; Hu, J.; Kwak, J.H.; Yang, Z.; Ren, R.; Markmaitree, T.; Shaw, L.L. Study the effects of mechanical activation on Li–N–H systems with 1H and 6Li solid-state NMR. *J. Power Sources* **2007**, *170*, 419–424. [CrossRef]
13. Shaw, L.L.; Ren, R.; Markmaitree, T.; Osborn, W. Effects of mechanical activation on dehydrogenation of the lithium amide and lithium hydride system. *J. Alloys Compd.* **2008**, *448*, 263–271. [CrossRef]
14. Osborn, W.; Markmaitree, T.; Shaw, L.L.; Hu, J.-Z.; Kwak, J.; Yang, Z. Low temperature milling of the $LiNH_2$ + LiH hydrogen storage system. *Int. J. Hydrogen Energy* **2009**, *34*, 4331–4339. [CrossRef]
15. Varin, R.; Jang, M.; Polanski, M. The effects of ball milling and molar ratio of LiH on the hydrogen storage properties of nanocrystalline lithium amide and lithium hydride ($LiNH_2$ + LiH) system. *J. Alloys Compd.* **2010**, *491*, 658–667. [CrossRef]
16. Varin, R.; Jang, M. The effects of graphite on the reversible hydrogen storage of nanostructured lithium amide and lithium hydride ($LiNH_2$ + 1.2LiH) system. *J. Alloys Compd.* **2011**, *509*, 7143–7151. [CrossRef]
17. Nayebossadri, S. Kinetic rate-limiting steps in dehydrogenation of Li–N–H and Li–Mg–N–H systems–effects of elemental Si and Al. *Int. J. Hydrogen Energy* **2011**, *36*, 8335–8343. [CrossRef]
18. Isobe, S.; Ichikawa, T.; Hanada, N.; Leng, H.Y.; Fichtner, M.; Fuhr, O.; Fujii, H. Effect of Ti catalyst with different chemical form on Li–N–H hydrogen storage properties. *J. Alloys Compd.* **2005**, *404–406*, 439–442. [CrossRef]
19. Nayebossadri, S.; Aguey-Zinsou, K.F.; Guo, Z.X. Effect of nitride additives on Li–N–H hydrogen storage system. *Int. J. Hydrogen Energy* **2011**, *36*, 7920–7926. [CrossRef]
20. Sale, M.; Pistidda, C.; Taras, A.; Napolitano, E.; Milanese, C.; Karimi, F.; Dornheim, M.; Garroni, S.; Enzo, S.; Mulas, G. In situ synchrotron radiation powder X-ray diffraction study of the $2LiNH_2$ + LiH + KBH_4 system. *J. Alloys Compd.* **2013**, *580* (Suppl. 1), S278–S281. [CrossRef]
21. Yao, J.H.; Shang, C.; Aguey-Zinsou, K.F.; Guo, Z.X. Desorption characteristics of mechanically and chemically modified $LiNH_2$ and ($LiNH_2$ + LiH). *J. Alloys Compd.* **2007**, *432*, 277–282. [CrossRef]
22. David, W.I.F.; Jones, M.O.; Gregory, D.H.; Jewell, C.M.; Johnson, S.R.; Walton, A.; Edwards, P.P. A Mechanism for Non-stoichiometry in the Lithium Amide/Lithium Imide Hydrogen Storage Reaction. *J. Am. Chem. Soc.* **2007**, *129*, 1594–1601. [CrossRef] [PubMed]
23. Pistidda, C.; Santoru, A.; Garroni, S.; Bergemann, N.; Rzeszutek, A.; Horstmann, C.; Thomas, D.; Klassen, T.; Dornheim, M. First Direct Study of the Ammonolysis Reaction in the Most Common Alkaline and Alkaline Earth Metal Hydrides by in Situ SR-PXD. *J. Phys. Chem. C* **2015**, *119*, 934–943. [CrossRef]

24. Makepeace, J.W.; Jones, M.O.; Callear, S.K.; Edwards, P.P.; David, W.I. In situ X-ray powder diffraction studies of hydrogen storage and release in the Li–N–H system. *Phys. Chem. Chem. Phys.* **2014**, *16*, 4061–4070. [CrossRef] [PubMed]
25. Anderson, P.A.; Chater, P.A.; Hewett, D.R.; Slater, P.R. Hydrogen storage and ionic mobility in amide-halide systems. *Faraday Discuss.* **2011**, *151*, 271–284. [CrossRef] [PubMed]
26. Matsuo, M.; Sato, T.; Miura, Y.; Oguchi, H.; Zhou, Y.; Maekawa, H.; Takamura, H.; Orimo, S.-I. Synthesis and lithium fast-ion conductivity of a new complex hydride $Li_3(NH_2)_2I$ with double-layered structure. *Chem. Mater.* **2010**, *22*, 2702–2704. [CrossRef]
27. Howard, M.A.; Clemens, O.; Slater, P.R.; Anderson, P.A. Hydrogen absorption and lithium ion conductivity in Li_6NBr_3. *J. Alloys Compd.* **2015**, *645* (Suppl. 1), S174–S177. [CrossRef]
28. Nguyen, T.T.T.; Reed, D.; Book, D.; Anderson, P.A. Hydrogen release and uptake in the Li–Zn–N system. *J. Alloys Compd.* **2015**, *645* (Suppl. 1), S295–S298. [CrossRef]
29. Davies, R.A.; Hewett, D.R.; Anderson, P.A. Enhancing ionic conductivity in lithium amide for improved energy storage materials. *Adv. Nat. Sci. Nanosci. Nanotechnol.* **2015**, *6*, 015005.
30. Davies, R.A.; Anderson, P.A. Synthesis and characterization of two new amide chloride compounds: Potential H_2 storage materials. *Int. J. Hydrogen Energy* **2015**, *40*, 3001–3005. [CrossRef]
31. Cao, H.; Wang, J.; Chua, Y.; Wang, H.; Wu, G.; Xiong, Z.; Qiu, J.; Chen, P. NH_3 Mediated or Ion Migration Reaction: The Case Study on Halide–Amide System. *J. Phys. Chem. C* **2014**, *118*, 2344–2349. [CrossRef]
32. Leng, H.; Wu, Z.; Duan, W.; Xia, G.; Li, Z. Effect of $MgCl_2$ additives on the H-desorption properties of Li–N–H system. *Int. J. Hydrogen Energy* **2012**, *37*, 903–907. [CrossRef]
33. Fernández Albanesi, L.; Arneodo Larochette, P.; Gennari, F.C. Destabilization of the $LiNH_2$–LiH hydrogen storage system by aluminum incorporation. *Int. J. Hydrogen Energy* **2013**, *38*, 12325–12334. [CrossRef]
34. Fernández Albanesi, L.; Garroni, S.; Arneodo Larochette, P.; Nolis, P.; Mulas, G.; Enzo, S.; Baró, M.D.; Gennari, F.C. Role of aluminum chloride on the reversible hydrogen storage properties of the Li–N–H system. *Int. J. Hydrogen Energy* **2015**, *40*, 13506–13517. [CrossRef]
35. Fernandez Albanesi, L.; Garroni, S.; Enzo, S.; Gennari, F.C. New amide-chloride phases in the Li-Al-N-H-Cl system: Formation and hydrogen storage behaviour. *Dalton Trans.* **2016**, *45*, 5808–5814. [CrossRef] [PubMed]
36. Dong, B.-X.; Gao, J.-J.; Tian, H.; Teng, Y.-L.; Wang, L.-Z.; Liu, W.-L. Hydrogen desorption improvement of the $LiNH_2$–LiH–KF composite. *Int. J. Hydrogen Energy* **2016**, *41*, 16122–16128. [CrossRef]
37. Zhang, W.; Wang, H.; Cao, H.; He, T.; Guo, J.; Wu, G.; Chen, P. Effects of doping $FeCl_3$ on hydrogen storage properties of Li-N-H system. *Prog. Nat. Sci. Mater. Int.* **2017**, *27*, 139–143. [CrossRef]
38. Amica, G.; Larochette, P.A.; Gennari, F. Hydrogen storage properties of $LiNH_2$–LiH system with MgH_2, CaH_2 and TiH_2 added. *Int. J. Hydrogen Energy* **2015**, *40*, 9335–9346. [CrossRef]
39. Lin, H.-J.; Li, H.-W.; Murakami, H.; Akiba, E. Remarkably improved hydrogen storage properties of $LiNH_2$-LiH composite via the addition of CeF_4. *J. Alloys Compd.* **2018**, *735*, 1017–1022. [CrossRef]
40. Chu, H.; Xiong, Z.; Wu, G.; He, T.; Wu, C.; Chen, P. Hydrogen storage properties of Li–Ca–N–H system with different molar ratios of $LiNH_2/CaH_2$. *Int. J. Hydrogen Energy* **2010**, *35*, 8317–8321. [CrossRef]
41. Meisner, G.P.; Scullin, M.L.; Balogh, M.P.; Pinkerton, F.E.; Meyer, M.S. Hydrogen Release from Mixtures of Lithium Borohydride and Lithium Amide: A Phase Diagram Study. *J. Phys. Chem. B* **2006**, *110*, 4186–4192. [CrossRef] [PubMed]
42. Nakamori, Y.; Ninomiya, A.; Kitahara, G.; Aoki, M.; Noritake, T.; Miwa, K.; Kojima, Y.; Orimo, S. Dehydriding reactions of mixed complex hydrides. *J. Power Sources* **2006**, *155*, 447–455. [CrossRef]
43. Tokoyoda, K.; Hino, S.; Ichikawa, T.; Okamoto, K.; Fujii, H. Hydrogen desorption/absorption properties of Li–Ca–N–H system. *J. Alloys Compd.* **2007**, *439*, 337–341. [CrossRef]
44. Xiong, Z.; Wu, G.; Hu, J.; Chen, P. Investigation on chemical reaction between $LiAlH_4$ and $LiNH_2$. *J. Power Sources* **2006**, *159*, 167–170. [CrossRef]
45. Zhang, Y.; Liu, Y.; Yang, Y.; Li, Y.; Hu, J.; Gao, M.; Pan, H. Superior catalytic activity of in situ reduced metallic Co for hydrogen storage in a $Co(OH)_2$-containing $LiBH_4/2LiNH_2$ composite. *Mater. Res. Bull.* **2018**, *97*, 544–552. [CrossRef]
46. Chu, H.; Xiong, Z.; Wu, G.; Guo, J.; He, T.; Chen, P. Improved dehydrogenation properties of $Ca(BH_4)_2$-$LiNH_2$ combined system. *Dalton Trans.* **2010**, *39*, 10585–10587. [CrossRef] [PubMed]
47. Makepeace, J.W.; David, W.I.F. Structural Insights into the Lithium Amide-Imide Solid Solution. *J. Phys. Chem. C* **2017**, *121*, 12010–12017. [CrossRef]

48. Leng, H.Y.; Ichikawa, T.; Hino, S.; Hanada, N.; Isobe, S.; Fujii, H. New Metal−N−H System Composed of $Mg(NH_2)_2$ and LiH for Hydrogen Storage. *J. Phys. Chem. B* **2004**, *108*, 8763–8765. [CrossRef]
49. Nakamori, Y.; Kitahara, G.; Orimo, S. Synthesis and dehydriding studies of Mg–N–H systems. *J. Power Sources* **2004**, *138*, 309–312. [CrossRef]
50. Orimo, S.; Nakamori, Y.; Kitahara, G.; Miwa, K.; Ohba, N.; Noritake, T.; Towata, S. Destabilization and enhanced dehydriding reaction of $LiNH_2$: An electronic structure viewpoint. *Appl. Phys. A* **2004**, *79*, 1765–1767. [CrossRef]
51. Luo, W. ($LiNH_2$-MgH_2): A viable hydrogen storage system. *J. Alloys Compd.* **2004**, *381*, 284–287. [CrossRef]
52. Xiong, Z.T.; Wu, G.T.; Hu, H.J.; Chen, P. Ternary imides for hydrogen storage. *Adv. Mater.* **2004**, *16*, 1522–1525. [CrossRef]
53. Chen, Y.; Wu, C.-Z.; Wang, P.; Cheng, H.-M. Structure and hydrogen storage property of ball-milled $LiNH_2/MgH_2$ mixture. *Int. J. Hydrogen Energy* **2006**, *31*, 1236–1240. [CrossRef]
54. Luo, W.; Sickafoose, S. Thermodynamic and structural characterization of the Mg–Li–N–H hydrogen storage system. *J. Alloys Compd.* **2006**, *407*, 274–281. [CrossRef]
55. Luo, W.; Stewart, K. Characterization of NH_3 formation in desorption of Li–Mg–N–H storage system. *J. Alloys Compd.* **2007**, *440*, 357–361. [CrossRef]
56. Luo, W.; Wang, J.; Stewart, K.; Clift, M.; Gross, K. Li-Mg-N-H: Recent investigations and development. *J. Alloys Compd.* **2007**, *446–447*, 336–341. [CrossRef]
57. Markmaitree, T.; Osborn, W.; Shaw, L.L. Comparisons between MgH_2-and LiH-containing systems for hydrogen storage applications. *Int. J. Hydrogen Energy* **2008**, *33*, 3915–3924. [CrossRef]
58. Leng, H.; Ichikawa, T.; Hino, S.; Hanada, N.; Isobe, S.; Fujii, H. Synthesis and decomposition reactions of metal amides in metal–N–H hydrogen storage system. *J. Power Sources* **2006**, *156*, 166–170. [CrossRef]
59. Dolci, F.; Napolitano, E.; Weidner, E.; Enzo, S.; Moretto, P.; Brunelli, M.; Hansen, T.; Fichtner, M.; Lohstroh, W. Magnesium imide: Synthesis and structure determination of an unconventional alkaline earth imide from decomposition of magnesium amide. *Inorg. Chem.* **2010**, *50*, 1116–1122. [CrossRef] [PubMed]
60. Rijssenbeek, J.; Gao, Y.; Hanson, J.; Huang, Q.; Jones, C.; Toby, B. Crystal structure determination and reaction pathway of amide–hydride mixtures. *J. Alloys Compd.* **2008**, *454*, 233–244. [CrossRef]
61. Yang, J.; Sudik, A.; Wolverton, C. Activation of hydrogen storage materials in the Li–Mg–N–H system: Effect on storage properties. *J. Alloys Compd.* **2007**, *430*, 334–338. [CrossRef]
62. Anton, D.L.; Price, C.J.; Gray, J. Affects of Mechanical Milling and Metal Oxide Additives on Sorption Kinetics of 1:1 $LiNH_2/MgH_2$ Mixture. *Energies* **2011**, *4*, 826–844. [CrossRef]
63. Bill, R.F.; Reed, D.; Book, D.; Anderson, P.A. Effect of the calcium halides, $CaCl_2$ and $CaBr_2$, on hydrogen desorption in the Li–Mg–N–H system. *J. Alloys Compd.* **2015**, *645*, S96–S99. [CrossRef]
64. Demirocak, D.E.; Srinivasan, S.S.; Ram, M.K.; Kuhn, J.N.; Muralidharan, R.; Li, X.; Goswami, D.Y.; Stefanakos, E.K. Reversible hydrogen storage in the Li–Mg–N–H system—The effects of Ru doped single walled carbon nanotubes on NH_3 emission and kinetics. *Int. J. Hydrogen Energy* **2013**, *38*, 10039–10049. [CrossRef]
65. Durojaiye, T.; Hayes, J.; Goudy, A. Rubidium hydride: An exceptional dehydrogenation catalyst for the lithium amide/magnesium hydride system. *J. Phys. Chem. C* **2013**, *117*, 6554–6560. [CrossRef]
66. Durojaiye, T.; Hayes, J.; Goudy, A. Potassium, rubidium and cesium hydrides as dehydrogenation catalysts for the lithium amide/magnesium hydride system. *Int. J. Hydrogen Energy* **2015**, *40*, 2266–2273. [CrossRef]
67. Hayes, J.; Durojaiye, T.; Goudy, A. Hydriding and dehydriding kinetics of RbH-doped $2LiNH_2/MgH_2$ hydrogen storage system. *J. Alloys Compd.* **2015**, *645* (Suppl. 1), S496–S499. [CrossRef]
68. Miyaoka, H.; Wang, Y.; Hino, S.; Isobe, S.; Tokoyoda, K.; Ichikawa, T.; Kojima, Y. Kinetic Modification on Hydrogen Desorption of Lithium Hydride and Magnesium Amide System. *Materials* **2015**, *8*, 3896–3909. [CrossRef] [PubMed]
69. Price, C.; Gray, J.; Lascola Jr, R.; Anton, D.L. The effects of halide modifiers on the sorption kinetics of the Li-Mg-N-H System. *Int. J. Hydrogen Energy* **2012**, *37*, 2742–2749. [CrossRef]
70. Sun, F.; Yan, M.-Y.; Ye, J.-H.; Liu, X.-P.; Jiang, L.-J. Effect of CO on hydrogen storage performance of KF doped $2LiNH_2 + MgH_2$ material. *J. Alloys Compd.* **2014**, *616*, 47–50. [CrossRef]
71. Ulmer, U.; Hu, J.; Franzreb, M.; Fichtner, M. Preparation, scale-up and testing of nanoscale, doped amide systems for hydrogen storage. *Int. J. Hydrogen Energy* **2013**, *38*, 1439–1449. [CrossRef]

72. Yan, M.Y.; Sun, F.; Liu, X.P.; Ye, J.H.; Yuan, H.P.; Wang, S.M.; Jiang, L.J. Experimental study on hydrogen storage properties of Li–Mg–N–H based tank. *J. Alloys Compd.* **2014**, *603*, 19–22. [CrossRef]
73. Luo, W.; Stavila, V.; Klebanoff, L.E. New insights into the mechanism of activation and hydrogen absorption of ($2LiNH_2$–MgH_2). *Int. J. Hydrogen Energy* **2012**, *37*, 6646–6652. [CrossRef]
74. Durojaiye, T.; Goudy, A. Desorption kinetics of lithium amide/magnesium hydride systems at constant pressure thermodynamic driving forces. *Int. J. Hydrogen Energy* **2012**, *37*, 3298–3304. [CrossRef]
75. Yang, J.; Sudik, A.; Siegel, D.J.; Halliday, D.; Drews, A.; Carter, R.O.; Wolverton, C.; Lewis, G.J.; Sachtler, J.W.A.; Low, J.J.; et al. Hydrogen storage properties of $2LiNH_2$+$LiBH_4$+MgH_2. *J. Alloys Compd.* **2007**, *446–447*, 345–349. [CrossRef]
76. Sudik, A.; Yang, J.; Halliday, D.; Wolverton, C. Hydrogen Storage Properties in $(LiNH_2)_2$-$LiBH_4$-(MgH_2)X Mixtures (X = 0.0–1.0). *J. Phys. Chem. C* **2008**, *112*, 4384–4390. [CrossRef]
77. Parviz, R.; Varin, R. Combined effects of molar ratio and ball milling energy on the phase transformations and mechanical dehydrogenation in the lithium amide-magnesium hydride ($LiNH_2$+ $nMgH_2$)(n = 0.5–2.0) nanocomposites. *Int. J. Hydrogen Energy* **2013**, *38*, 8313–8327. [CrossRef]
78. Varin, R.; Parviz, R.; Polanski, M.; Wronski, Z. The effect of milling energy input and molar ratio on the dehydrogenation and thermal conductivity of the ($LiNH_2$+ $nMgH_2$)(n = 0.5, 0.7, 0.9, 1.0, 1.5 and 2.0) nanocomposites. *Int. J. Hydrogen Energy* **2014**, *39*, 10585–10599. [CrossRef]
79. Xiong, Z.; Hu, J.; Wu, G.; Chen, P.; Luo, W.; Gross, K.; Wang, J. Thermodynamic and kinetic investigations of the hydrogen storage in the Li–Mg–N–H system. *J. Alloys Compd.* **2005**, *398*, 235–239. [CrossRef]
80. Xiong, Z.; Wu, G.; Hu, J.; Chen, P.; Luo, W.; Wang, J. Investigations on hydrogen storage over Li–Mg–N–H complex—The effect of compositional changes. *J. Alloys Compd.* **2006**, *417*, 190–194. [CrossRef]
81. Aoki, M.; Noritake, T.; Kitahara, G.; Nakamori, Y.; Towata, S.; Orimo, S. Dehydriding reaction of $Mg(NH_2)_2$–LiH system under hydrogen pressure. *J. Alloys Compd.* **2007**, *428*, 307–311. [CrossRef]
82. Hu, J.; Fichtner, M. Formation and stability of ternary imides in the Li−Mg−N−H hydrogen storage system. *Chem. Mater.* **2009**, *21*, 3485–3490. [CrossRef]
83. Ikeda, S.; Tokoyoda, K.; Kiyobayashi, T.; Kuriyama, N. Cyclic properties and ammonia by-product emission of Li/Mg–N–H hydrogen storage material. *Int. J. Hydrogen Energy* **2011**, *36*, 8373–8380. [CrossRef]
84. Cao, H.; Chua, Y.; Zhang, Y.; Xiong, Z.; Wu, G.; Qiu, J.; Chen, P. Releasing 9.6 wt% of H_2 from $Mg(NH_2)_2$–3LiH–NH_3BH_3 through mechanochemical reaction. *Int. J. Hydrogen Energy* **2013**, *38*, 10446–10452. [CrossRef]
85. Liu, Y.; Hu, J.; Xiong, Z.; Wu, G.; Chen, P. Improvement of the hydrogen-storage performances of Li–Mg–N–H system. *J. Mater. Res.* **2007**, *22*, 1339–1345. [CrossRef]
86. Sudik, A.; Yang, J.; Halliday, D.; Wolverton, C. Kinetic Improvement in the $Mg(NH_2)_2$−LiH Storage System by Product Seeding. *J. Phys. Chem. C* **2007**, *111*, 6568–6573. [CrossRef]
87. Liu, Y.; Zhong, K.; Luo, K.; Gao, M.; Pan, H.; Wang, Q. Size-Dependent Kinetic Enhancement in Hydrogen Absorption and Desorption of the Li−Mg−N−H System. *J. Am. Chem. Soc.* **2009**, *131*, 1862–1870. [CrossRef] [PubMed]
88. Janot, R.; Eymery, J.-B.; Tarascon, J.-M. Investigation of the processes for reversible hydrogen storage in the Li–Mg–N–H system. *J. Power Sources* **2007**, *164*, 496–502. [CrossRef]
89. Li, C.; Liu, Y.; Ma, R.; Zhang, X.; Li, Y.; Gao, M.; Pan, H. Superior Dehydrogenation/Hydrogenation Kinetics and Long-Term Cycling Performance of K and Rb Cocatalyzed $Mg(NH_2)_2$–2LiH system. *ACS Appl. Mater. Interfaces* **2014**, *6*, 17024–17033. [CrossRef] [PubMed]
90. Liang, C.; Liu, Y.; Wei, Z.; Jiang, Y.; Wu, F.; Gao, M.; Pan, H. Enhanced dehydrogenation/hydrogenation kinetics of the $Mg(NH_2)_2$–2LiH system with NaOH additive. *Int. J. Hydrogen Energy* **2011**, *36*, 2137–2144. [CrossRef]
91. Ma, L.-P.; Dai, H.-B.; Liang, Y.; Kang, X.-D.; Fang, Z.-Z.; Wang, P.-J.; Wang, P.; Cheng, H.-M. Catalytically enhanced hydrogen storage properties of $Mg(NH_2)_2$ + 2LiH material by graphite-supported Ru nanoparticles. *J. Phys. Chem. C* **2008**, *112*, 18280–18285. [CrossRef]
92. Shahi, R.R.; Yadav, T.; Shaz, M.; Srivastva, O. Studies on dehydrogenation characteristic of $Mg(NH_2)_2$/LiH mixture admixed with vanadium and vanadium based catalysts (V, V_2O_5 and VCl_3). *Int. J. Hydrogen Energy* **2010**, *35*, 238–246. [CrossRef]

93. Wang, J.; Liu, T.; Wu, G.; Li, W.; Liu, Y.; Araújo, C.M.; Scheicher, R.H.; Blomqvist, A.; Ahuja, R.; Xiong, Z.; et al. Potassium-Modified $Mg(NH_2)_2$/2LiH System for Hydrogen Storage. *Angew. Chem. Int. Ed.* **2009**, *48*, 5828–5832. [CrossRef] [PubMed]
94. Yan, M.-Y.; Sun, F.; Liu, X.-P.; Ye, J.-H. Effects of compaction pressure and graphite content on hydrogen storage properties of $Mg(NH_2)_2$–2LiH hydride. *Int. J. Hydrogen Energy* **2014**, *39*, 19656–19661. [CrossRef]
95. Torre, F.; Valentoni, A.; Milanese, C.; Pistidda, C.; Marini, A.; Dornheim, M.; Enzo, S.; Mulas, G.; Garroni, S. Kinetic improvement on the CaH_2-catalyzed $Mg(NH_2)_2$+2LiH system. *J. Alloys Compd.* **2015**, *645*, S284–S287. [CrossRef]
96. Hu, J.; Liu, Y.; Wu, G.; Xiong, Z.; Chua, Y.S.; Chen, P. Improvement of Hydrogen Storage Properties of the Li–Mg–N–H System by Addition of $LiBH_4$. *Chem. Mater.* **2008**, *20*, 4398–4402. [CrossRef]
97. Napolitano, E.; Dolci, F.; Campesi, R.; Pistidda, C.; Hoelzel, M.; Moretto, P.; Enzo, S. Crystal structure solution of $KMg(ND)(ND_2)$: An ordered mixed amide/imide compound. *Int. J. Hydrogen Energy* **2014**, *39*, 868–876. [CrossRef]
98. Santoru, A.; Garroni, S.; Pistidda, C.; Milanese, C.; Girella, A.; Marini, A.; Masolo, E.; Valentoni, A.; Bergemann, N.; Le, T.T.; et al. A new potassium-based intermediate and its role in the desorption properties of the K-Mg-N-H system. *Phys. Chem. Chem. Phys.* **2016**, *18*, 3910–3920. [CrossRef] [PubMed]
99. Santoru, A.; Pistidda, C.; Sorby, M.H.; Chierotti, M.R.; Garroni, S.; Pinatel, E.; Karimi, F.; Cao, H.; Bergemann, N.; Le, T.T.; et al. KNH_2-KH: A metal amide-hydride solid solution. *Chem. Commun.* **2016**, *52*, 11760–11763. [CrossRef] [PubMed]
100. Wang, J.; Chen, P.; Pan, H.; Xiong, Z.; Gao, M.; Wu, G.; Liang, C.; Li, C.; Li, B.; Wang, J. Solid–Solid Heterogeneous Catalysis: The Role of Potassium in Promoting the Dehydrogenation of the $Mg(NH_2)_2$/2LiH Composite. *ChemSusChem* **2013**, *6*, 2181–2189. [CrossRef] [PubMed]
101. Wang, J.; Wu, G.; Chua, Y.S.; Guo, J.; Xiong, Z.; Zhang, Y.; Gao, M.; Pan, H.; Chen, P. Hydrogen Sorption from the $Mg(NH_2)_2$-KH System and Synthesis of an Amide–Imide Complex of $KMg(NH)(NH_2)$. *ChemSusChem* **2011**, *4*, 1622–1628. [CrossRef] [PubMed]
102. Li, C.; Liu, Y.; Yang, Y.; Gao, M.; Pan, H. High-temperature failure behaviour and mechanism of K-based additives in Li-Mg-N-H hydrogen storage systems. *J. Mater. Chem. A* **2014**, *2*, 7345–7353. [CrossRef]
103. Liang, C.; Liu, Y.; Gao, M.; Pan, H. Understanding the role of K in the significantly improved hydrogen storage properties of a KOH-doped Li-Mg-N-H system. *J. Mater. Chem. A* **2013**, *1*, 5031–5036. [CrossRef]
104. Liu, Y.; Li, C.; Li, B.; Gao, M.; Pan, H. Metathesis Reaction-Induced Significant Improvement in Hydrogen Storage Properties of the KF-Added $Mg(NH_2)_2$–2LiH System. *J. Phys. Chem. C* **2013**, *117*, 866–875. [CrossRef]
105. Liu, Y.; Yang, Y.; Zhang, X.; Li, Y.; Gao, M.; Pan, H. Insights into the dehydrogenation reaction process of a K-containing $Mg(NH_2)_2$–2LiH system. *Dalton Trans.* **2015**, *44*, 18012–18018. [CrossRef] [PubMed]
106. Lin, H.-J.; Li, H.-W.; Paik, B.; Wang, J.; Akiba, E. Improvement of hydrogen storage property of three-component $Mg(NH_2)_2$-$LiNH_2$-LiH composites by additives. *Dalton Trans.* **2016**, *45*, 15374–15381. [CrossRef] [PubMed]
107. Li, C.; Liu, Y.; Gu, Y.; Gao, M.; Pan, H. Improved Hydrogen-Storage Thermodynamics and Kinetics for an RbF-Doped $Mg(NH_2)_2$–2LiH System. *Chem. Asian J.* **2013**, *8*, 2136–2143. [CrossRef] [PubMed]
108. Santoru, A.; Pistidda, C.; Brighi, M.; Chierotti, M.R.; Heere, M.; Karimi, F.; Cao, H.; Capurso, G.; Chaudhary, A.-L.; Gizer, G.; et al. Insights into the Rb–Mg–N–H System: An Ordered Mixed Amide/Imide Phase and a Disordered Amide/Hydride Solid Solution. *Inorg. Chem.* **2018**, *57*, 3197–3205. [CrossRef] [PubMed]
109. Zhang, J.; Liu, Y.; Zhang, X.; Yang, Y.; Zhang, Q.; Jin, T.; Wang, Y.; Gao, M.; Sun, L.; Pan, H. Synthesis of CsH and its effect on the hydrogen storage properties of the $Mg(NH_2)_2$–2LiH system. *Int. J. Hydrogen Energy* **2016**, *41*, 11264–11274. [CrossRef]
110. Zhang, J.; Wang, Y.; Zhang, M.; Leng, Z.; Gao, M.; Hu, J.; Liu, Y.; Pan, H. Improved overall hydrogen storage properties of a CsH and KH co-doped $Mg(NH_2)_2$/2LiH system by forming mixed amides of Li-K and Cs-Mg. *RSC Adv.* **2017**, *7*, 30357–30364. [CrossRef]
111. Xia, G.; Chen, X.; Zhao, Y.; Li, X.; Guo, Z.; Jensen, C.M.; Gu, Q.; Yu, X. High-Performance Hydrogen Storage Nanoparticles Inside Hierarchical Porous Carbon Nanofibers with Stable Cycling. *ACS Appl. Mater. Interfaces* **2017**, *9*, 15502–15509. [CrossRef] [PubMed]
112. Vajo, J.J.; Skeith, S.L.; Mertens, F. Reversible Storage of Hydrogen in Destabilized $LiBH_4$. *J. Phys. Chem. B* **2005**, *109*, 3719–3722. [CrossRef] [PubMed]

113. Filinchuk, Y.E.; Yvon, K.; Meisner, G.P.; Pinkerton, F.E.; Balogh, M.P. On the Composition and Crystal Structure of the New Quaternary Hydride Phase $Li_4BN_3H_{10}$. *Inorg. Chem.* **2006**, *45*, 1433–1435. [CrossRef] [PubMed]
114. Lewis, G.J.; Sachtler, J.W.A.; Low, J.J.; Lesch, D.A.; Faheem, S.A.; Dosek, P.M.; Knight, L.M.; Halloran, L.; Jensen, C.M.; Yang, J.; et al. High throughput screening of the ternary $LiNH_2$–MgH_2–$LiBH_4$ phase diagram. *J. Alloys Compd.* **2007**, *446–447*, 355–359. [CrossRef]
115. Sudik, A.; Yang, J.; Siegel, D.J.; Wolverton, C.; Carter, R.O.; Drews, A.R. Impact of Stoichiometry on the Hydrogen Storage Properties of $LiNH_2-LiBH_4-MgH_2$ Ternary Composites. *J. Phys. Chem. C* **2009**, *113*, 2004–2013. [CrossRef]
116. Yang, J.; Sudik, A.; Siegel, D.J.; Halliday, D.; Drews, A.; Carter, R.O.; Wolverton, C.; Lewis, G.J.; Sachtler, J.W.A.; Low, J.J.; et al. A Self-Catalyzing Hydrogen-Storage Material. *Angew. Chem. Int. Ed.* **2008**, *47*, 882–887. [CrossRef] [PubMed]
117. Hu, J.; Fichtner, M.; Chen, P. Investigation on the Properties of the Mixture Consisting of $Mg(NH_2)_2$, LiH, and $LiBH_4$ as a Hydrogen Storage Material. *Chem. Mater.* **2008**, *20*, 7089–7094. [CrossRef]
118. Hu, J.; Weidner, E.; Hoelzel, M.; Fichtner, M. Functions of $LiBH_4$ in the hydrogen sorption reactions of the 2LiH-$Mg(NH_2)_2$ system. *Dalton Trans.* **2010**, *39*, 9100–9107. [CrossRef] [PubMed]
119. Cao, H.J.; Wu, G.T.; Zhang, Y.; Xiong, Z.T.; Qiu, J.S.; Chen, P. Effective thermodynamic alteration to $Mg(NH_2)_2$-LiH system: Achieving near ambient-temperature hydrogen storage. *J. Mater. Chem. A* **2014**, *2*, 15816–15822. [CrossRef]
120. Wang, H.; Cao, H.J.; Wu, G.T.; He, T.; Chen, P. The improved Hydrogen Storage Performances of the Multi-Component Composite: $2Mg(NH_2)_2$-3LiH-$LiBH_4$. *Energies* **2015**, *8*, 6898–6909. [CrossRef]
121. Wang, H.; Cao, H.J.; Pistidda, C.; Garroni, S.; Wu, G.T.; Klassen, T.; Dorheim, M.; Chen, P. Effects of Stoichiometry on the H-2-Storage Properties of $Mg(NH_2)_2$-LiH-$LiBH_4$ Tri-Component Systems. *Chem. Asian J.* **2017**, *12*, 1758–1764. [CrossRef] [PubMed]
122. Wang, H.; Wu, G.T.; Cao, H.J.; Pistidda, C.; Chaudhary, A.L.; Garroni, S.; Dornheim, M.; Chen, P. Near Ambient Condition Hydrogen Storage in a Synergized Tricomponent Hydride System. *Adv. Energy Mater.* **2017**, *7*. [CrossRef]
123. Wang, H.; Cao, H.; Zhang, W.; Chen, J.; Wu, H.; Pistidda, C.; Ju, X.; Zhou, W.; Wu, G.; Etter, M.; et al. Li_2NH-$LiBH_4$: A Complex Hydride with Near Ambient Hydrogen Adsorption and Fast Lithium Ion Conduction. *Chem. Eur. J.* **2018**, *24*, 1342–1347. [CrossRef] [PubMed]
124. Wolczyk, A.; Paik, B.; Sato, T.; Nervi, C.; Brighi, M.; GharibDoust, S.P.; Chierotti, M.; Matsuo, M.; Li, G.; Gobetto, R.; et al. $Li_5(BH_4)3NH$: Lithium-Rich Mixed Anion Complex Hydride. *J. Phys. Chem. C* **2017**, *121*, 11069–11075. [CrossRef]
125. Zhan, L.; Zhang, Y.; Zhuang, X.; Fang, H.; Zhu, Y.; Guo, X.; Chen, J.; Wang, Z.; Li, L. Ionic conductivities of lithium borohydride-lithium nitride composites. *Solid State Ion.* **2017**, *304*, 150–155. [CrossRef]
126. Chen, P.; Xiong, Z.T.; Yang, L.F.; Wu, G.T.; Luo, W.F. Mechanistic investigations on the heterogeneous solid-state reaction of magnesium amides and lithium hydrides. *J. Phys. Chem. B* **2006**, *110*, 14221–14225. [CrossRef] [PubMed]
127. Cao, H.; Wang, H.; He, T.; Wu, G.; Xiong, Z.; Qiu, J.; Chen, P. Improved kinetics of the $Mg(NH_2)_2$–2LiH system by addition of lithium halides. *RSC Adv.* **2014**, *4*, 32555–32561. [CrossRef]
128. Matsuo, M.; Remhof, A.; Martelli, P.; Caputo, R.; Ernst, M.; Miura, Y.; Sato, T.; Oguchi, H.; Maekawa, H.; Takamura, H.; et al. Complex Hydrides with (BH_4)- and (NH_2)-Anions as New Lithium Fast-Ion Conductors. *J. Am. Chem. Soc.* **2009**, *131*, 16389–16391. [CrossRef] [PubMed]
129. Srinivasan, S.S.; Niemann, M.U.; Hattrick-Simpers, J.R.; McGrath, K.; Sharma, P.C.; Goswami, D.Y.; Stefanakos, E.K. Effects of nano additives on hydrogen storage behavior of the multinary complex hydride $LiBH_4/LiNH_2/MgH_2$. *Int. J. Hydrogen Energy* **2010**, *35*, 9646–9652. [CrossRef]
130. Zhang, X.; Li, Z.; Lv, F.; Li, H.; Mi, J.; Wang, S.; Liu, X.; Jiang, L. Improved hydrogen storage performance of the $LiNH_2$–MgH_2–$LiBH_4$ system by addition of ZrCo hydride. *Int. J. Hydrogen Energy* **2010**, *35*, 7809–7814. [CrossRef]
131. Hu, J.; Pohl, A.; Wang, S.; Rothe, J.; Fichtner, M. Additive Effects of $LiBH_4$ and $ZrCoH_3$ on the Hydrogen Sorption of the Li-Mg-N-H Hydrogen Storage System. *J. Phys. Chem. C* **2012**, *116*, 20246–20253. [CrossRef]

132. Yuan, H.; Zhang, X.; Li, Z.; Ye, J.; Guo, X.; Wang, S.; Liu, X.; Jiang, L. Influence of metal oxide on $LiBH_4/2LiNH_2/MgH_2$ system for hydrogen storage properties. *Int. J. Hydrogen Energy* **2012**, *37*, 3292–3297. [CrossRef]
133. Zhao, W.; Jiang, L.; Wu, Y.; Ye, J.; Yuan, B.; Li, Z.; Liu, X.; Wang, S. Improved dehydrogenation cycle performance of the $1.1MgH_2$–$2LiNH_2$–$0.1LiBH_4$ system by addition of $LaNi_{4.5}Mn_{0.5}$ alloy. *J. Rare Earths* **2015**, *33*, 783–790. [CrossRef]
134. Li, Z.-N.; Qiu, H.-C.; Guo, X.-M.; Ye, J.-H.; Wang, S.-M.; Jiang, L.-J.; Du, J.; Cuevas, F. Hydrogen storage properties of Li–Mg–N–B–H/$ZrCoH_3$ composite with different ball-milling atmospheres. *Rare Metals* **2017**, 1–7. [CrossRef]
135. Cao, H.; Zhang, W.; Pistidda, C.; Puszkiel, J.; Milanese, C.; Santoru, A.; Karimi, F.; Castro Riglos, M.V.; Gizer, G.; Welter, E.; et al. Kinetic alteration of the $6Mg(NH_2)_2$–9LiH-$LiBH_4$ system by co-adding YCl_3 and Li_3N. *Phys. Chem. Chem. Phys.* **2017**, *19*, 32105–32115. [CrossRef] [PubMed]
136. Bürger, I.; Hu, J.J.; Vitillo, J.G.; Kalantzopoulos, G.N.; Deledda, S.; Fichtner, M.; Baricco, M.; Linder, M. Material properties and empirical rate equations for hydrogen sorption reactions in $2LiNH_2$–$1.1MgH_2$–$0.1LiBH_4$–3wt.% $ZrCoH_3$. *Int. J. Hydrogen Energy* **2014**, *39*, 8283–8292. [CrossRef]
137. Bürger, I.; Luetto, C.; Linder, M. Advanced reactor concept for complex hydrides: Hydrogen desorption at fuel cell relevant boundary conditions. *Int. J. Hydrogen Energy* **2014**, *39*, 7346–7355. [CrossRef]
138. Baricco, M.; Bang, M.; Fichtner, M.; Hauback, B.; Linder, M.; Luetto, C.; Moretto, P.; Sgroi, M. SSH2S: Hydrogen storage in complex hydrides for an auxiliary power unit based on high temperature proton exchange membrane fuel cells. *J. Power Sources* **2017**, *342*, 853–860. [CrossRef]
139. Yang, J.; Li, D.; Fu, H.; Xin, G.; Zheng, J.; Li, X. In situ hybridization of $LiNH_2$-LiH-$Mg(BH_4)_2$ nano-composites: Intermediate and optimized hydrogenation properties. *Phys. Chem. Chem. Phys.* **2012**, *14*, 2857–2863. [CrossRef] [PubMed]
140. Pan, H.; Shi, S.; Liu, Y.; Li, B.; Yang, Y.; Gao, M. Improved hydrogen storage kinetics of the Li-Mg-N-H system by addition of $Mg(BH_4)_2$. *Dalton Trans.* **2013**, *42*, 3802–3811. [CrossRef] [PubMed]
141. Qiu, S.; Ma, X.; Wang, E.; Chu, H.; Huot, J.; Zou, Y.; Xiang, C.; Xu, F.; Sun, L. Enhanced hydrogen storage properties of $2LiNH_2/MgH_2$ through the addition of $Mg(BH_4)_2$. *J. Alloys Compd.* **2017**, *704*, 44–50. [CrossRef]
142. Li, B.; Liu, Y.; Gu, J.; Gu, Y.; Gao, M.; Pan, H. Mechanistic investigations on significantly improved hydrogen storage performance of the $Ca(BH_4)_2$-added $2LiNH_2/MgH_2$ system. *Int. J. Hydrogen Energy* **2013**, *38*, 5030–5038. [CrossRef]
143. Amica, G.; Cova, F.; Arneodo Larochette, P.; Gennari, F.C. Effective participation of $Li_4(NH_2)3BH_4$ in the dehydrogenation pathway of the $Mg(NH_2)_2$–2LiH composite. *Phys. Chem. Chem. Phys.* **2016**, *18*, 17997–18005. [CrossRef] [PubMed]
144. Amica, G.; Cova, F.; Arneodo Larochette, P.; Gennari, F.C. Two-controlling mechanisms model for hydrogen desorption in the $Li_4(NH_2)3BH_4$ doped $Mg(NH_2)_2$–2LiH system. *Int. J. Hydrogen Energy* **2017**, *42*, 6127–6136. [CrossRef]
145. Shukla, V.; Bhatnagar, A.; Soni, P.K.; Vishwakarma, A.K.; Shaz, M.A.; Yadav, T.P.; Srivastava, O.N. Enhanced hydrogen sorption in a Li-Mg-N-H system by the synergistic role of $Li_4(NH_2)3BH_4$ and $ZrFe_2$. *Phys. Chem. Chem. Phys.* **2017**, *19*, 9444–9456. [CrossRef] [PubMed]
146. Gamba, N.S.; Amica, G.; Arneodo Larochette, P.; Gennari, F.C. Interaction between $Li_2Mg(NH)_2$ and CO: Effect on the hydrogen storage behavior of the $Li_4(NH_2)_3BH_4$ doped $Mg(NH_2)_2$–2LiH composite. *Int. J. Hydrogen Energy* **2017**, *42*, 6024–6032. [CrossRef]
147. Cao, H.J.; Richter, T.M.M.; Pistidda, C.; Chaudhary, A.L.; Santoru, A.; Gizer, G.; Niewa, R.; Chen, P.; Klassen, T.; Dornheim, M. Ternary Amides Containing Transition Metals for Hydrogen Storage: A Case Study with Alkali Metal Amidozincates. *Chemsuschem* **2015**, *8*, 3777–3782. [CrossRef] [PubMed]
148. Cao, H.J.; Santoru, A.; Pistidda, C.; Richter, T.M.M.; Chaudhary, A.L.; Gizer, G.; Niewa, R.; Chen, P.; Klassen, T.; Dornheim, M. New synthesis route for ternary transition metal amides as well as ultrafast amide-hydride hydrogen storage materials. *Chem. Commun.* **2016**, *52*, 5100–5103. [CrossRef] [PubMed]
149. Cao, H.J.; Pistidda, C.; Richter, T.M.M.; Santoru, A.; Milanese, C.; Garroni, S.; Bednarcik, J.; Chaudhary, A.L.; Gizer, G.; Liermann, H.P.; et al. In Situ X-ray Diffraction Studies on the De/rehydrogenation Processes of the K-2 $Zn(NH_2)_4$-8LiH System. *J. Phys. Chem. C* **2017**, *121*, 1546–1551. [CrossRef]

150. Jepsen, L.H.; Wang, P.; Wu, G.; Xiong, Z.; Besenbacher, F.; Chen, P.; Jensen, T.R. Thermal decomposition of sodium amide, $NaNH_2$, and sodium amide hydroxide composites, $NaNH_2$-NaOH. *Phys. Chem. Chem. Phys.* **2016**, *18*, 25257–25264. [CrossRef] [PubMed]
151. Jain, A.; Miyaoka, H.; Ichikawa, T. Two-Peak Mystery of $LiNH_2$–NaH Dehydrogenation Is Solved? A Study of the Analogous Sodium Amide/Lithium Hydride System. *J. Phys. Chem. C* **2016**, *120*, 27903–27909. [CrossRef]
152. Sheppard, D.A.; Paskevicius, M.; Buckley, C.E. Hydrogen Desorption from the $NaNH_2-MgH_2$ System. *J. Phys. Chem. C* **2011**, *115*, 8407–8413. [CrossRef]
153. Dolotko, O.; Paulson, N.; Pecharsky, V.K. Thermochemical transformations in $2MNH_2$–$3MgH_2$ systems (M = Li or Na). *Int. J. Hydrogen Energy* **2010**, *35*, 4562–4568. [CrossRef]
154. Yamaguchi, S.; Miyaoka, H.; Ichikawa, T.; Kojima, Y. Thermal decomposition of sodium amide. *Int. J. Hydrogen Energy* **2017**, *42*, 5213–5219. [CrossRef]
155. Garroni, S.; Delogu, F.; Bonatto Minella, C.; Pistidda, C.; Cuesta-Lopez, S. Mechanically activated metathesis reaction in $NaNH_2$–MgH_2 powder mixtures. *J. Mater. Sci.* **2017**, *52*, 11891–11899. [CrossRef]
156. Pireddu, G.; Valentoni, A.; Minella, C.B.; Pistidda, C.; Milanese, C.; Enzo, S.; Mulas, G.; Garroni, S. Comparison of the thermochemical and mechanochemical transformations in the $2NaNH_2$–MgH_2 system. *Int. J. Hydrogen Energy* **2015**, *40*, 1829–1835. [CrossRef]
157. Singh, N.K.; Kobayashi, T.; Dolotko, O.; Wiench, J.W.; Pruski, M.; Pecharsky, V.K. Mechanochemical transformations in $NaNH_2$-MgH_2 mixtures. *J. Alloys Compd.* **2012**, *513*, 324–327. [CrossRef]
158. Xiong, Z.; Hu, J.; Wu, G.; Chen, P. Hydrogen absorption and desorption in Mg–Na–N–H system. *J. Alloys Compd.* **2005**, *395*, 209–212. [CrossRef]
159. Jain, A.; Kumar, S.; Miyaoka, H.; Zhang, T.; Isobe, S.; Ichikawa, T.; Kojima, Y. Ammonia suppression during decomposition of sodium amide by the addition of metal hydride. *Int. J. Hydrogen Energy* **2017**, *42*, 22388–22394. [CrossRef]
160. Morelle, F.; Jepsen, L.H.; Jensen, T.R.; Sharma, M.; Hagemann, H.; Filinchuk, Y. Reaction Pathways in $Ca(BH_4)_2$–$NaNH_2$ and $Mg(BH_4)_2$–$NaNH_2$ Hydrogen-Rich Systems. *J. Phys. Chem. C* **2016**, *120*, 8428–8435. [CrossRef]
161. Bai, Y.; Zhao, L.-L.; Wang, Y.; Liu, X.; Wu, F.; Wu, C. Light-weight $NaNH_2$–$NaBH_4$ hydrogen storage material synthesized via liquid phase ball milling. *Int. J. Hydrogen Energy* **2014**, *39*, 13576–13582. [CrossRef]
162. Wu, C.; Bai, Y.; Yang, J.-h.; Wu, F.; Long, F. Characterizations of composite $NaNH_2$–$NaBH_4$ hydrogen storage materials synthesized via ball milling. *Int. J. Hydrogen Energy* **2012**, *37*, 889–893. [CrossRef]
163. Pei, Z.-W.; Wu, C.; Bai, Y.; Liu, X.; Wu, F. $NaNH_2$–$NaBH_4$ hydrogen storage composite materials synthesized via liquid phase ball-milling: Influence of Co–Ni–B catalyst on the dehydrogenation performances. *Int. J. Hydrogen Energy* **2017**, *42*, 14725–14733. [CrossRef]
164. Lu, J.; Fang, Z.Z. Dehydrogenation of a Combined $LiAlH_4/LiNH_2$ System. *J. Phys. Chem. B* **2005**, *109*, 20830–20834. [CrossRef] [PubMed]
165. Jepsen, L.H.; Wang, P.; Wu, G.; Xiong, Z.; Besenbacher, F.; Chen, P.; Jensen, T.R. Synthesis and decomposition of $Li_3Na(NH_2)_4$ and investigations of Li-Na-N-H based systems for hydrogen storage. *Phys. Chem. Chem. Phys.* **2016**, *18*, 1735–1742. [CrossRef] [PubMed]
166. Chua, Y.S.; Wu, G.; Xiong, Z.; Chen, P. Investigations on the solid state interaction between $LiAlH_4$ and $NaNH_2$. *J. Solid State Chem.* **2010**, *183*, 2040–2044. [CrossRef]
167. Dolotko, O.; Zhang, H.; Ugurlu, O.; Wiench, J.W.; Pruski, M.; Scott Chumbley, L.; Pecharsky, V. Mechanochemical transformations in $Li(Na)AlH_4$–$Li(Na)NH_2$ systems. *Acta Mater.* **2007**, *55*, 3121–3130. [CrossRef]

© 2018 by the authors. Licensee MDPI, Basel, Switzerland. This article is an open access article distributed under the terms and conditions of the Creative Commons Attribution (CC BY) license (http://creativecommons.org/licenses/by/4.0/).